

Targeted transcriptional downregulation of MYC using epigenomic controllers demonstrates antitumor activity in hepatocellular carcinoma models

Received: 26 September 2023

Accepted: 29 August 2024

Published online: 16 September 2024

 Check for updates

William Senapedis¹✉, Kayleigh M. Gallagher^{1,2}, Elmer Figueroa^{1,3}, Jeremiah D. Farelli¹, Robert Lyng^{1,4}, J. Graeme Hodgson¹, Charles W. O'Donnell¹, Joseph V. Newman¹, Madison Pacaro¹, Stephen K. Siecinski¹, Justin Chen¹ & Thomas G. McCauley¹

Dysregulation of master regulator c-MYC (MYC) plays a central role in hepatocellular carcinoma (HCC) and other cancers but remains an elusive target for therapeutic intervention. *MYC* expression is epigenetically modulated within naturally occurring DNA loop structures, Insulated Genomic Domains (IGDs). We present a therapeutic approach using an epigenomic controller (EC), a programmable epigenomic mRNA medicine, to precisely modify *MYC* IGD sub-elements, leading to methylation of *MYC* regulatory elements and durable downregulation of *MYC* mRNA transcription. Significant antitumor activity is observed in preclinical models of HCC treated with the MYC-targeted EC, as monotherapy or in combination with tyrosine kinase or immune checkpoint inhibitors. These findings pave the way for clinical development of MYC-targeting epigenomic controllers in HCC patients and provide a framework for programmable epigenomic mRNA therapeutics for cancer and other diseases.

The c-MYC (MYC) oncogene is a pleiotropic transcription factor (TF) that plays a central role in regulating the activity of tumor cells and the tumor microenvironment, driving initiation and maintenance of the tumor ecosystem. MYC inhibition in preclinical mouse models can elicit regression of established tumors *in vivo*^{1–3}, mediated through a variety of distinct mechanisms including tumor cell proliferative arrest, senescence, and apoptosis, disruption of tumor-associated vascular- and stromal-cell activities, and prevention of immune evasion^{4–7}. Interestingly, while systemic MYC inhibition in adult mice also elicits inhibitory effects on normal regenerating tissues such as the intestinal and haematopoietic systems, these effects are generally well tolerated and reversible, even though antitumor activity is maintained^{8,9}. The differential responses to MYC inhibition of tumor tissue versus normal regenerative tissues provide an attractive

opportunity to develop MYC inhibitors with potentially safe and effective therapeutic profiles in cancer patients.

Development of targeted MYC inhibitors has proven elusive, in part, because the MYC protein lacks a structured binding pocket that can be effectively targeted by small molecule inhibitors^{4,10,11}. Further, the short-lived expression of MYC mRNA and protein, combined with the multitude of oncogenic inputs that drive chronic *MYC* gene expression in tumor cells^{4,12}, suggest that direct inhibition of the MYC transcript or protein would require maintaining effective drug exposures for sustained periods to offset the autoregulation of MYC expression in cancer cells.

To address these challenges, we have leveraged a platform for gene control based on controlled epigenomic modulation of Insulated Genomic Domains (IGDs), which offers the potential to selectively and

¹Omega Therapeutics, Cambridge, MA, USA. ²Present address: AstraZeneca, Waltham, MA, USA. ³Present address: Flagship Pioneering, Cambridge, MA, USA.

⁴Present address: Saliogen Therapeutics, Lexington, MA, USA. ✉ e-mail: wsenapedis@omegatx.com

durably downregulate *MYC* gene expression. IGDs are ubiquitous naturally occurring chromatin loop structures, conserved throughout mammalian genomes to compartmentalize and operationalize the vast amounts of information found in DNA^{13–15}. IGDs enable targeted control of gene transcription via rapid, environmentally responsive epigenetic mechanisms. The evolutionary function of IGD loops is to bring genes and cis-regulatory elements into close proximity, activating or repressing transcription via multiple chromatin elements: loop anchors, such as those mediated by factors including CTCF, and cis-regulatory elements, such as enhancers and gene promoters^{13,14,16}. *MYC* is located within a well-characterized IGD¹⁷, with transcriptional levels controlled by diverse regulatory elements, making it an attractive target that is sensitive to epigenetic control.

Others have shown epigenetic downregulation of *MYC* mRNA using nuclease-deficient CRISPR-associated protein 9 (dCas9) fused to effector domains targeting specific regulatory sequences in the *MYC* locus^{17,18}. For example, a fusion of dCas9 to the DNA methyltransferase DNMT3A-3L promotes methylation of a CTCF-binding site upstream of *MYC* and decreases *MYC* expression in cultured tumor cells¹⁷. A fusion of dCasX to KRAB targeting the *MYC* promoter reduces *MYC* expression, inhibits growth and migration, triggers apoptosis in cultured bladder cancer cells, and decreases the mass of xenograft tumors in mice¹⁸. Results from these studies offer promise that epigenetic downregulation of *MYC* could form a class of cancer therapeutics.

We have developed a dual-repressor, *MYC*-targeted epigenomic controller, OTX-2002, that downregulates *MYC* expression and is in early phase clinical development (NCT05497453). In preclinical proof-of-concept studies, we describe the effects of controlled pre-transcriptional downregulation of *MYC* through epigenetic mechanisms using in vitro and in vivo models of HCC. Our results demonstrate the potential for clinical development of OTX-2002 as a monotherapy as well as in combination with HCC standard of care (SoC) agents, including both tyrosine kinase and immune checkpoint inhibitors.

Results

Design of OTX-2002-DS for specific and durable downregulation of *MYC*

We sought to develop a drug product that epigenetically downregulates *MYC* in hepatic tumors. To achieve this goal, we took an approach to the design and delivery of our drug substance (DS; the mRNA) that differs from previously described systems for epigenetic downregulation of *MYC* using CRISPR/dCas^{17,18}. We engineered a bicistronic mRNA, OTX-2002-DS, that controls *MYC* mRNA expression (Fig. 1A). This epigenetic repressor system includes two proteins that contain zinc finger (ZF)-based DNA binding domains fused to effector domains that act via different epigenetic mechanisms at distinct genomic sites. Given the variety of mechanisms of epigenetic regulation, we reasoned that a system employing multiple distinct mechanisms of repression would be more effective at downregulating *MYC* and inhibiting growth of cancer cells and be less susceptible to adaptive resistance. Moreover, because ZF DNA binding domains, unlike CRISPR-based polypeptides, have intrinsic DNA binding activity, OTX-2002-DS is independently active and does not require guide RNAs to be provided as separate components. Consequently, OTX-2002-DS is a simple, single, compact drug substance that can readily be packaged in LNPs for systemic in vivo delivery.

The first cistron (Cistron 1) of OTX-2002-DS is engineered to express a protein, MYC epigenomic controller element 1 (MYC-EC-E1), comprising a ZF DNA binding domain protein targeted to the region surrounding the *MYC* promoter, tethered to an effector domain, MQ1, a well-characterized bacterial DNA methyltransferase protein isolated from *Mollicutes spiroplasma* (M. Sss1), strain MQ1^{19,20}. We selected MQ1 owing to its smaller coding size and its ability to methylate CpG dinucleotides effectively and selectively without being subject to multimeric effects from exogenous human DNMT fusions²¹.

This effector methylates CpG dinucleotides, impacting TF binding as well as local compaction of chromatin, leading to decreased *MYC* gene expression. The second cistron (Cistron 2) is engineered to express a protein, MYC epigenomic controller element 2 (MYC-EC-E2), comprising a ZF DNA binding domain protein targeted to a key enhancer docking anchor site upstream of the *MYC* transcriptional start site¹⁷, tethered to a Krüppel-associated box repressor (KRAB) protein effector domain. The KRAB domains recruit proteins to induce histone H3 lysine 9 trimethylation (H3K9me3), a critical epigenetic mark contributing to constitutive heterochromatin formation and transcriptional silencing, and impairment of *MYC* activation via enhancer looping²².

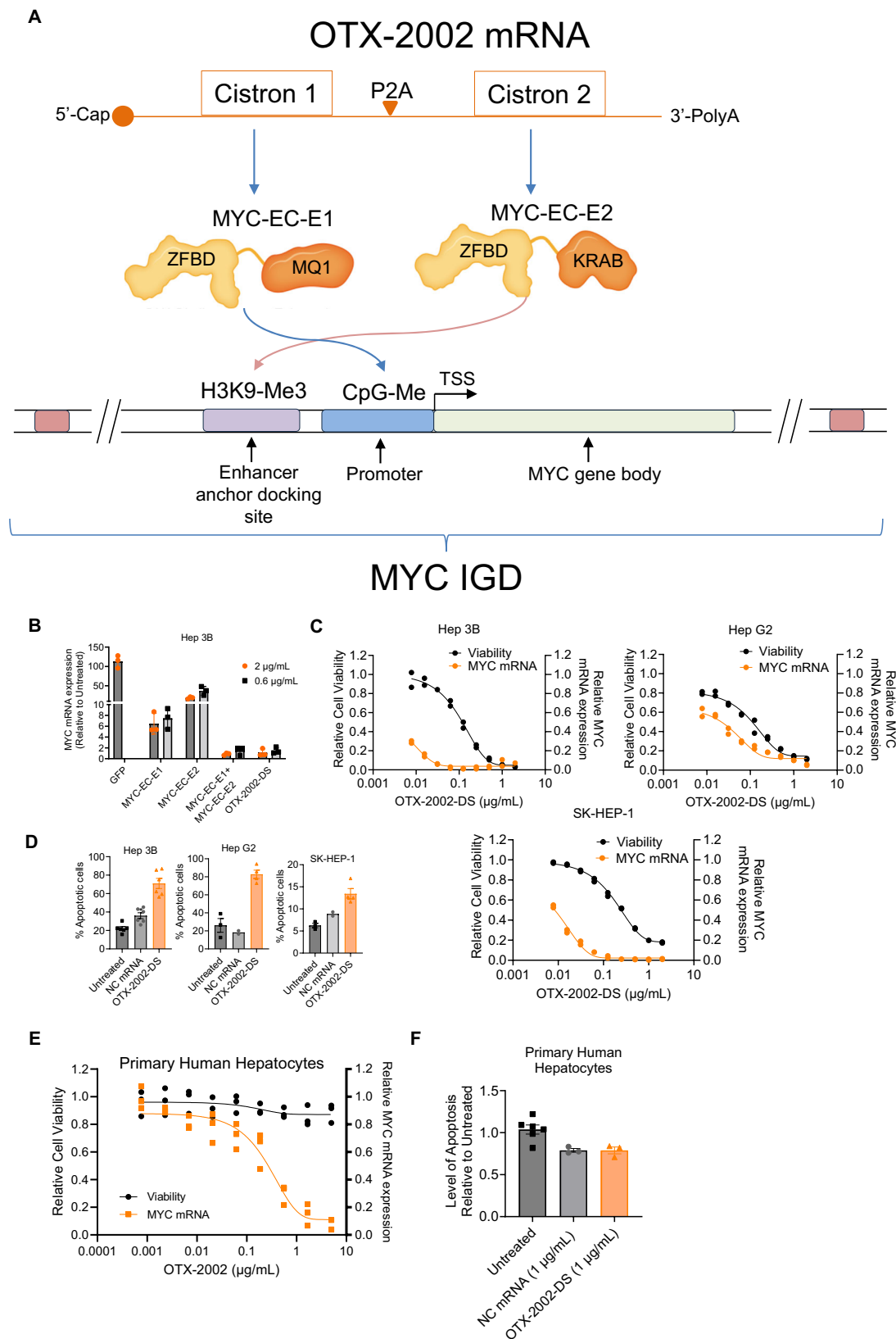
OTX-2002-DS selectively inhibits HCC cell viability compared to normal hepatocytes

To evaluate the impact of MYC-EC-E1 and MYC-EC-E2 on HCC tumor cells, a series of in vitro assays were conducted using several mRNAs engineered to express human influenza hemagglutinin (HA)-tagged versions of MYC-EC-E1 and MYC-EC-E2, formulated in tool lipid nanoparticles (LNPs) MC3 or SSOP (see methods for details). Initially, the Hep 3B HCC cell line was utilized to support the rationale for development of OTX-2002-DS for more potent downregulation of *MYC* expression. Hep 3B was transfected with HA-tagged versions of MYC-EC-E1, MYC-EC-E2, or both (either by co-transfection with individual mRNAs or by transfection with OTX-2002-DS). Co-transfection with both single cistronic mRNAs or the bicistronic OTX-2002-DS significantly downregulated *MYC* relative to either mRNA alone (Fig. 1B), supporting the rationale for development of OTX-2002-DS for more potent downregulation of *MYC* expression. Additional HCC cell lines were selected to represent two of the three major HCC tumor subtypes, S1 and S2, associated with more aggressive phenotypes and a higher risk of early recurrence in HCC patients²³. The S1 subtype is characterized by aberrant TGF- β activation of the WNT signaling pathway, leading to the overexpression of *MYC*²³. The S2 subtype is characterized by proliferation gene signatures as well as *MYC* and *AKT* activation²⁴. Knockdown of *MYC* in these cell lines has been associated with loss of viability both in vitro and in vivo^{25–28}. OTX-2002-DS potently inhibited viability of all HCC cell lines tested, associated with downregulation of *MYC* mRNA expression (Fig. 1C, S1A). To delineate the mechanism of decreased cell viability, induction of apoptosis following OTX-2002-DS treatment was evaluated in HCC cell lines by Annexin V/PI staining 48 h after treatment. A 2–3-fold increase in apoptosis was observed across all cell lines relative to cells treated with negative control mRNA (Fig. 1D, S1B).

In contrast, Acuitas Therapeutics' drug product OTX-2002 did not inhibit viability (Fig. 1E) or induce apoptosis (Figs. 1F, S1C) of primary human hepatocytes (PHH) at concentrations that induced *MYC* downregulation to levels observed in HCC cells. Hep 3B and PHH were similarly transfectable when using luciferase mRNA in Acuitas Therapeutics' LNP (Fig. S2), indicating that the effect of increased activity on HCC cells compared to PHH is not due to significant transfection level differences. These data suggest that OTX-2002-induced *MYC* downregulation selectively inhibits viability of HCC cells with aggressive subtypes (S1 and S2), but not normal cells (PHH), mediated in part through induction of apoptosis.

OTX-2002-DS induces epigenetic modification of the *MYC* IGD leading to durable repression of *MYC* and selective repression of hallmark *MYC* gene expression signatures

To decipher the relationship between the kinetics of OTX-2002 epigenomic controller elements (MYC-EC-E1 and MYC-EC-E2), target engagement, and *MYC* gene expression changes, we conducted in vitro studies in the HCC cell lines Hep 3B and SK-HEP-1. HCC cells were transfected with OTX-2002-DS where the translated proteins were HA-tagged and quantifiable via western blot. The peak levels of MYC-EC-E1



and MYC-EC-E2 were reached at 6 h and were undetectable by 48 h (Figs. 2A, S3A). This was associated with increased CpG methylation at the targeted loci within the *MYC* IGD at 24 h which was sustained at 48 h (Fig. 2B) despite clearance of MYC-EC-E1 by 48 h (Figs. 2A, S3A), indicating that the CpG methylation marks were maintained at least to 48 h following degradation of MYC-EC-E2. Similarly, strong H3K9me3

methylation marks were observed at the *MYC* IGD 24 h after transfection (Fig. 2C) despite evidence of a decrease in MYC-EC-E2 expression by 24 h (Figs. 2A, S3A).

We next performed a time course study to evaluate *MYC* mRNA, *MYC* protein, DNA methylation at the *MYC* promoter, and cell viability following OTX-2002-DS treatment of Hep 3B and SK-HEP-1 cells.

Fig. 1 | Mechanism of action of OTX-2002 in HCC cell lines. **A** Bicistronic OTX-2002 mRNA encoding two bifunctional fusion proteins, MYC Epigenomic Controller-Element 1 (MYC-EC-E1) and Element 2 (MYC-EC-E2), target regulatory elements in the MYC Insulated Genomic Domain (IGD). Red boxes depict CCCTC-Binding factor (CTCF) binding sites of the looping IGD. Further details are available in the main text and ref. 17. **B** In vitro evaluation (at 48 h) of MYC-EC-E1 and MYC-EC-E2 alone or in combination compared to GFP mRNA in Hep 3B cells. Results are from one independent experiment ($n = 3$ technical replicates) and were repeated once. **C** Dose response of MYC mRNA expression and cell viability at 72 h of OTX-2002-DS treatment in three HCC cell lines. Results are from one independent experiment ($n = 2$ technical replicates per concentration) and were repeated once. **D** Annexin V/PI staining (gating strategy Fig. S1B) showing percentage of apoptotic cells in HCC cell lines treated with either negative control

(NC) mRNA or OTX-2002-DS for 48 h. Results are from one independent experiment (Hep 3B, $n = 6$ technical replicates for all groups; Hep G2 and SK-HEP-1, $n = 3$ technical replicates for untreated, $n = 2$ technical replicates for NC mRNA, $n = 4$ technical replicates for OTX-2002-DS) and were repeated once. **E** Dose response of MYC mRNA expression and cell viability at 72 h of OTX-2002 treatment in primary human hepatocytes (PHH). Results are from one independent experiment ($n = 3$ technical replicates) and were repeated once. **F** PS: Annexin V binding showing relative luminescence of apoptotic PHH after 48 h of treatment. Results are from one independent experiment ($n = 6$ technical replicates for untreated, $n = 3$ technical replicates for NC mRNA and OTX-2002-DS) and were repeated once. For all relevant panels error bars represent mean (\pm) standard error of the mean (SEM). Source data are provided as a Source Data file.

Whereas cells treated with negative control (non-coding mRNA) formulated in the same LNP did not show evident changes over the 96 h time course for any of the markers (Figs. 2D, E, S3D, S3E), OTX-2002-DS treatment led to a clear reduction in MYC mRNA and MYC protein within 6 h of treatment and complete loss of both by 24 h, which was maintained throughout the 96 h time course (Figs. 2D, E, S3B, S3C). DNA methylation was also detected as early as 6 h in this experiment and maintained at 96 h. This loss of MYC was associated with a reduction in HCC cell viability as early as 24 h and a near complete loss of viability by 72 h (Fig. 2D, E). These results are consistent with previous reports supporting a causal role for MYC in driving viability of HCC tumor cells^{25,27,28}. We further explored the durability of MYC mRNA downregulation at a dose of OTX-2002-DS that did not induce complete loss of cell viability. This experiment not only demonstrates repression of MYC mRNA up to 15 days post-treatment but also maintenance of DNA methylation throughout (Fig. 2F). Finally, we assessed the selectivity of MYC suppression with OTX-2002-DS treatment by evaluating global transcriptome changes by RNA-seq in PHH and Hep 3B tumor cells 24 h after treatment. As expected, given the central role for MYC in transcriptional regulation, 619 and 306 significantly ($\text{Padj} < 0.05$) and differentially expressed genes (>2 -fold up or down) were observed in PHH and Hep 3B cells, respectively (Fig. S3F). However, Gene Set Enrichment Analysis (GSEA) applied against MsigDB's 50 "hallmark" biological signatures, representing well-defined biological states²⁹, revealed that the only significantly altered biological signatures were downregulated MYC-specific hallmark signatures in both cell types (Fig. 2G, orange dots). Together these results suggest that MYC epigenomic controller elements encoded within OTX-2002 were translated intracellularly and exerted selective epigenomic modifications at the MYC locus within hours of treatment, leading to durable downregulation of MYC and subsequent loss of viability of HCC cells.

In HCC xenograft models, OTX-2002 reduces tumor burden, increases MYC gene methylation, and decreases MYC expression

To evaluate the effects of OTX-2002-DS in vivo we encapsulated it in an LNP formulation that is known to target liver tissue when administered systemically³⁰. To confirm delivery to liver and to liver-derived HCC tumors with this formulation, we encapsulated a luciferase-expressing mRNA construct in the Acuitas LNP (Fig. S2) and assessed luciferase activity by whole body imaging of mice bearing Hep 3B HCC subcutaneous xenografts. As expected, luciferase activity was observed in mouse liver and in HCC xenograft tissue (Fig. S4A). The latter observation suggests that liver-derived HCC tumors retain features of the cell of origin that enable LNP uptake outside of the target organ following systemic administration.

We next evaluated antitumor activity of OTX-2002 (LNP-encapsulated untagged OTX-2002-DS) in vivo. OTX-2002 was administered systemically via intravenous (IV) tail-vein injection once every 5 days (Q5D) to nude mice bearing subcutaneous Hep 3B tumors. We selected

a Q5D dosing regimen as a strategy to balance the sustained MYC epigenomic changes and MYC downregulation in tumor cells (Figs. 2F and S4B) while maximizing tumor cell transfection in vivo through repeated dosing and minimizing non-specific tolerability challenges associated with repeated IV dosing via mouse tail vein. OTX-2002 treatment led to a dose-proportional inhibition of tumor growth, which was significantly greater relative to mice treated with LNP-encapsulated negative control (NC) mRNA (Fig. 3A). Antitumor responses at the lowest OTX-2002 dose tested (0.3 mg/kg) were comparable to treatment with sorafenib at a standard preclinical dose and regimen (50 mg/kg, once daily PO). All dose levels tested were well tolerated (Fig. 3B, C)—no mice were taken off study prior to study termination due to body weight loss or overall disposition and no dose holds or dose reductions were required. Similar results were observed in Hep G2 and SK-HEP-1 subcutaneous xenograft models (Fig. S4C, S4D). Tumor growth inhibition in Hep 3B tumors was associated with dose-proportional increases in methylation at the MYC IGD locus (Fig. 3D) and a dose-proportional decrease in MYC protein expression via IHC (Figs. 3D, S5). Further, in OTX-2002 treated mice, IHC showed dose-proportional increase in expression of the apoptosis marker caspase-3, and dose-proportional decreases in the proliferation marker Ki-67 and the HCC-specific tumor marker alpha-fetoprotein (AFP) (Figs. 3D, S5).

Next, we tested OTX-2002 antitumor activity in an orthotopic HCC model comprised of luciferase-tagged Hep 3B cells injected into mouse liver, the primary tissue target site of the LNP formulation used in these studies. Consistent with observations in subcutaneously implanted Hep 3B tumors, OTX-2002 in this orthotopic model resulted in a significant decrease in tumor burden relative to mice treated with negative control (Fig. 3E). Again, OTX-2002 treatment was well tolerated at the efficacious doses tested—no mice were taken off study prior to study termination due to body weight loss (Fig. 3F, G) or overall disposition and no dose holds or dose reductions were required. Collectively, these results suggested that systemic administration of OTX-2002, at well-tolerated doses, resulted in delivery of functional mRNA to HCC tumor tissue growing within distinct sites (subcutaneous and liver) leading to MYC IGD methylation, MYC downregulation, and tumor growth inhibition mediated, in part, by induction of apoptosis and inhibition of proliferation of tumor cells.

OTX-2002 enhances the activity of tyrosine kinase inhibitors in vitro and in vivo models of HCC

Sorafenib³¹ and lenvatinib³² are approved for treatment of unresectable HCC and exert antitumor effects through inhibition of multiple tyrosine kinases that drive proliferation and survival of tumor cells and vascular endothelial cells^{33,34}. MYC is a critical downstream mediator of tyrosine kinase activation, which can be repressed by sorafenib treatment^{35,36} (Figs. 3D, S5) and has been implicated in mediating resistance to a broad range of TKIs, including sorafenib resistance in HCC^{35,37,38}. We therefore evaluated the ability

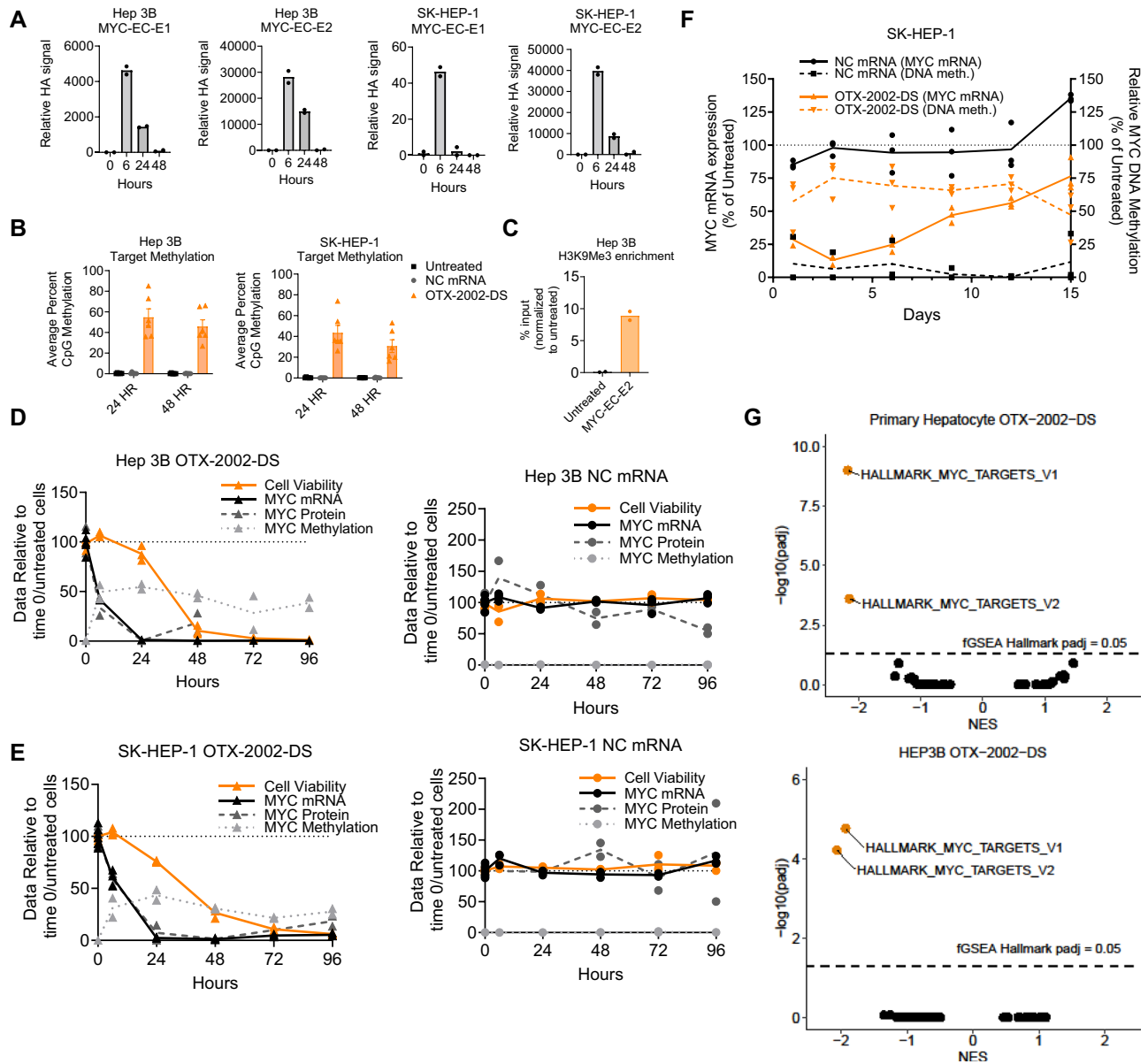


Fig. 2 | OTX-2002 increases epigenetic modification and reduces MYC expression. **A** Western blot quantification of HA-MYC-EC-E1 and HA-MYC-EC-E2 proteins. Results are from one independent experiment ($n = 2$ technical replicates) and were repeated once. **B** DNA methylation at the MYC-EC-E1 target site. Results are from one independent experiment ($n = 6$ technical replicates) and were repeated once. **C** ChIP-qPCR analysis at the MYC-EC-E2 target site (24 h). Results are from one independent experiment ($n = 2$ technical replicates) and were repeated once. **D** Time course results from one independent experiment ($n = 6$ technical replicates for untreated MYC mRNA and cell viability, $n = 5$ technical replicates for untreated MYC protein, $n = 3$ technical replicates for NC mRNA and OTX-2002 treated MYC mRNA and cell viability, $n = 2$ technical replicates for untreated MYC methylation, NC mRNA and OTX-2002 treated MYC protein and methylation) and were repeated once. **E** Time course results from one independent experiment ($n = 6$ technical replicates for untreated MYC mRNA and cell viability, $n = 4$ technical replicates for untreated MYC protein, $n = 3$ technical replicates for NC mRNA and OTX-2002 treated MYC mRNA and cell viability, $n = 2$ technical replicates for untreated MYC

promoter methylation, NC mRNA and OTX-2002 treated MYC protein and promoter methylation) and were repeated once. **F** Evaluation of single treatment over 15 days. Results are from one independent experiment ($n = 3$ technical replicates) and were repeated once. **G** GSEA results when tested against all Hallmark gene sets in PHH and Hep 3B cells after 24-h treatment. NES indicates directional association between RNA-seq data and gene set (negative=inhibition); $-\log_{10}(\text{padj})$ indicates significance of association with a threshold of $\text{padj} < 0.01$. DESeq2 identified differentially expressed genes using Wald test statistics and the Benjamini-Hochberg (BH) method to correct for multiple testing. The sorted test statistics were input to fGSEA with the Hallmark gene set (MSigDB). A permutation test of the input list estimated significant enrichment and the BH method accounted for multiple testing with a significant adjusted $p < 0.05$. Results are from one independent experiment and were repeated once. For all relevant panels error bars represent mean \pm standard error of the mean (SEM). Source data are provided as a Source Data file.

of OTX-2002 to enhance the activity of lenvatinib (Fig. 4) or sorafenib (Fig. S6) in HCC models in vitro and in vivo. In Hep 3B and SK-HEP-1 cells in vitro, the combination of the HA-tagged version of OTX-2002-DS with sorafenib or lenvatinib demonstrated additive and synergistic effects across the drug concentrations tested (Figs. 4A, S6A, Table 1). In Hep 3B subcutaneous xenografts in vivo, the

combinations of OTX-2002 plus lenvatinib or sorafenib resulted in significantly enhanced tumor growth inhibition relative to single agent treatment at tolerated doses (Figs. 4B–E, S6B–E). Collectively, these results indicated that OTX-2002-mediated downregulation of MYC enhances the antitumor activity of lenvatinib and sorafenib in preclinical models of HCC.

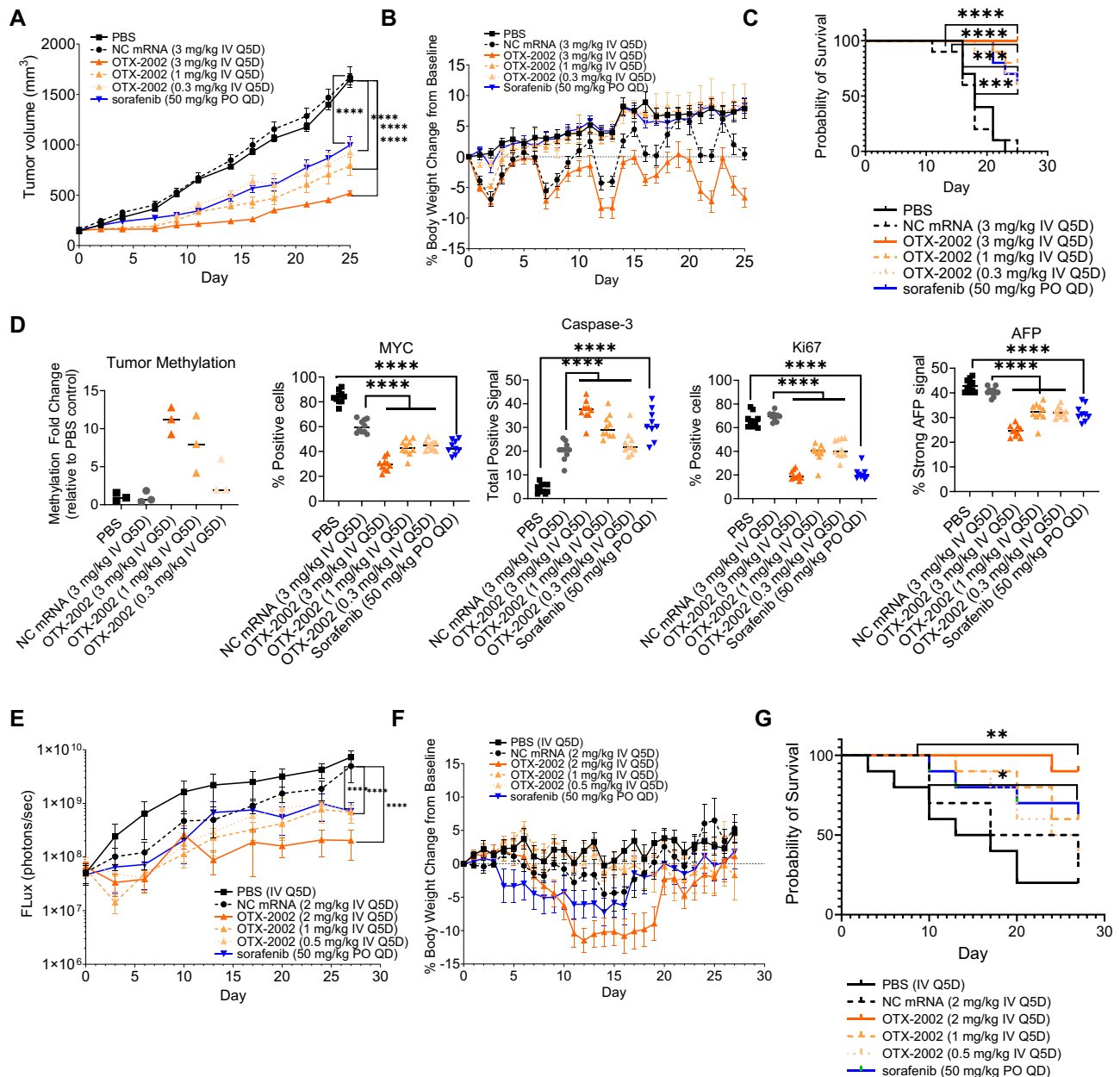


Fig. 3 | OTX-2002 reduces tumor burden and MYC expression in HCC xenograft models. **A** OTX-2002 in vivo efficacy as evaluated in Hep 3B subcutaneous xenografts in nude mice. Mice were administered treatment via intravenous injection (IV) once daily every five days (Q5D) or orally (PO) once daily (QD). Significance measured using two-way ANOVA comparing negative control (NC) mRNA to OTX-2002 treatments or PBS to sorafenib with adjusted *p* values for multiple comparisons; *****P* < 0.0001. Results are from one independent experiment (*n* = 10 mice per group) and were repeated once. **B** Body weight changes over the course of the Hep 3B study in (A). **C** Survival curves for Hep 3B study in (A) with mice removed when they reached an arbitrary endpoint of >1000 mm³. Significance measured using Log-rank (Mantel-Cox) test comparing NC mRNA to OTX-2002 treatment (*****P* < 0.0001 or ****P* = 0.0002) or PBS to sorafenib (****P* = 0.0001). **D** Targeted methylation sequencing from extracted tumors at the end of study in (A) (*n* = 3 tumors per group). IHC Quantification for staining with MYC, Caspase-3, Ki67, and

AFP (*n* = 10 mice per group except for sorafenib group where *n* = 9 mice). Significance measured using one-way ANOVA comparing NC mRNA to OTX-2002 or PBS to sorafenib with adjusted *p*-values for multiple comparisons; *****P* < 0.0001. **E** OTX-2002 in vivo efficacy evaluated in orthotopic xenografts of luciferase-expressing Hep 3B cells in nude mice. Significance measured using two-way ANOVA comparing NC mRNA to OTX-2002 treatment or PBS to sorafenib with adjusted *p*-values for multiple comparisons; *****P* < 0.0001. Results are from one independent experiment (*n* = 10 mice per group) and were repeated once. **F** Bodyweight change over course of the orthotopic study in (E). **G** Survival curves for Hep 3B orthotopic study in (E) with mice removed when they reached an arbitrary endpoint of FLux >10⁹. Significance measured using Log-rank (Mantel-Cox) test comparing NC mRNA to OTX-2002 at 2 mg/kg Q5D (**P* = 0.0064) or PBS to sorafenib (**P* = 0.0397). For all relevant panels error bars represent mean ± standard error of the mean (SEM). Source data are provided as a Source Data file.

MYC-targeted epigenomic controllers enhance the activity of anti-PD-1 and anti-PD-L1 immune checkpoint inhibitors in immune-competent syngeneic HCC models in vivo

Multiple immune checkpoint inhibitors are indicated for the treatment of HCC including PD-1 antibodies pembrolizumab³⁹ and nivolumab⁴⁰,

and PD-L1 antibody atezolizumab⁴¹. Inactivation of MYC is known to downregulate immune checkpoint PD-L1 on tumor cells leading to an immune response against these tumor cells^{42,43}. Targeted downregulation of MYC therefore represents a potential strategy for restoration of host immune response against tumors, as well as an

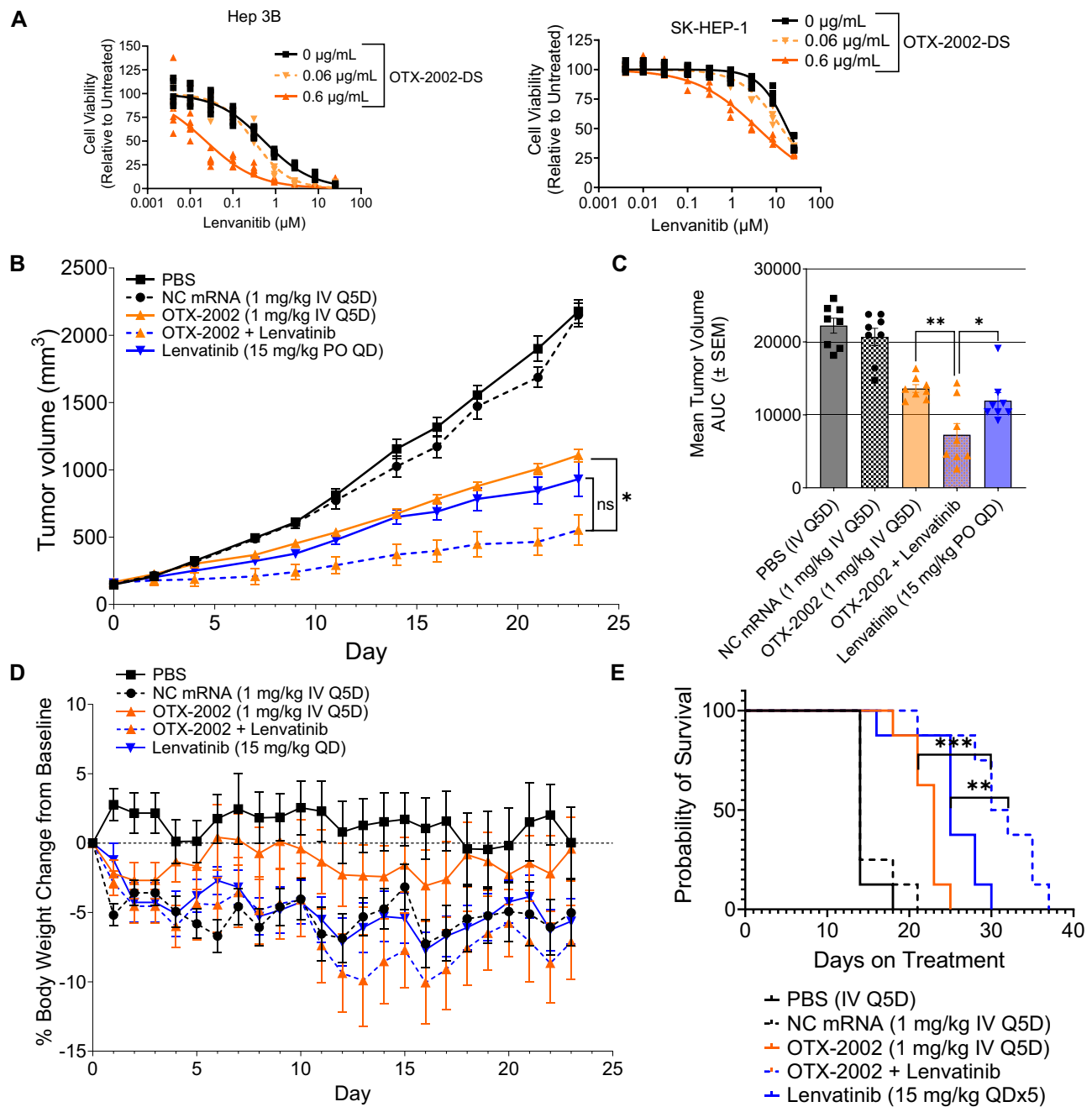


Fig. 4 | OTX-2002 exhibits combinatorial efficacy with standard of care tyrosine kinase inhibitors, lenvatinib, in HCC. A The effect of OTX-2002 on the lenvatinib response in HCC was evaluated through in vitro dose response studies of lenvatinib with increasing concentrations of HA-tagged OTX-2002-DS evaluated in Hep 3B (left) and SK-HEP-1 (right) cells. Results are from one independent experiment (Hep 3B, $n = 6$ technical replicates for all treatments; SK-HEP-1, $n = 6$ technical replicates for lenvatinib alone and combination with 0.06 μg/mL of OTX-2002, $n = 4$ technical replicates for lenvatinib combination with 0.6 μg/mL of OTX-2002) and were repeated once. **B–E** In vivo study using Hep 3B subcutaneous tumors to test combination of OTX-2002 plus lenvatinib. Hep 3B subcutaneous (B) tumor volume (two-way ANOVA with adjusted p -values for multiple comparisons; * $P = 0.0162$ and

ns = not significant) and (C) area under the curve (AUC; one-way ANOVA with adjusted p -value for multiple comparisons; ** $P = 0.0019$ and * $P = 0.0493$) at the noted treatment conditions. Results are from one independent experiment ($n = 8$ mice per group) and were repeated once. **D** Bodyweight changes over course of the combination study in (B). **E** Survival curves for combination study in (B) with mice removed when they reached an endpoint of >1000 mm³. Significance measured using Log-rank (Mantel-Cox) test comparing OTX-2002 (** $P = 0.001$) or lenvatinib (** $P = 0.0089$) single agents to combination group. For all relevant panels error bars represent mean \pm standard error of the mean (SEM). Source data are provided as a Source Data file.

approach to potentiating the effect of immune checkpoint inhibitors⁴⁴. To evaluate the effect of OTX-2002 on tumor cell PD-L1 expression, HCC tumor cells were cultured in vitro with interferon gamma (IFN- γ) to induce surface expression of PD-L1. Treatment with the HA-tagged version of OTX-2002-DS blocked the IFN- γ -driven induction of surface PD-L1 expression in both Hep 3B and SK-HEP-1 HCC cells (Fig. 5A, S7A,

B), suggesting that MYC repression by OTX-2002-DS may enhance antitumor activity by reactivating T-cell mediated tumor cell killing through the PD-L1/PD-1 axis.

We next evaluated the potential for epigenomic controller downregulation of *Myc* to enhance antitumor activity of immune checkpoint inhibitors in a syngeneic mouse HCC tumor model

Table 1 | OTX-2002 plus Lenvatinib IC₅₀ Calculations and Bliss Synergy Scores for Hep 3B and SK-HEP-1

Hep 3B			SK-HEP-1		
OTX-2002-DS Dose	Lenvatinib IC ₅₀	Bliss Synergy Score	OTX-2002-DS Dose	Lenvatinib IC ₅₀	Bliss Synergy Score
0 µg/mL	0.533 µM	5.37	0 µg/mL	17.69 µM	12.77
0.06 µg/mL	0.309 µM		0.06 µg/mL	13.28 µM	
0.6 µg/mL	0.023 µM		0.6 µg/mL	3.857 µM	

(Hepa1.6). To accomplish this, a mouse specific *Myc*-targeting epigenomic controller was generated (muMyc-EC) that expresses a murine surrogate HA-tagged version of the OTX-2002-DS controller element MYC-EC-E1 and selectively binds to mouse *Myc* IGD elements (Fig. 1A). Treatment of the Hepa1.6 mouse HCC cell line in vitro with muMyc-EC resulted in the expected decrease in *Myc* mRNA and increase in *Myc* methylation at the target *Myc* IGD site (Fig. 5B). LNP-encapsulated muMyc-EC, and murine surrogate anti-PD-1 or anti-PD-L1 antibodies, were administered alone or in combination to normal immunocompetent mice bearing subcutaneous Hepa1.6 syngeneic tumors. While each single agent treatment resulted in significant inhibition of tumor growth relative to PBS and negative control mice (treated with green fluorescent protein [GFP] mRNA) at well-tolerated doses, the combinations of muMyc-EC with anti-PD-L1 or anti-PD-1 antibodies at the same doses resulted in significantly enhanced inhibition of tumor growth relative to each single agent (Figs. 5C, D, S7C). In an additional study, fresh tumors were extracted after several doses of muMyc-EC and anti-PD-1 (single agents or in combination) to investigate immune infiltration (Fig. 5E). Extracted tumors were analyzed by flow cytometry for immune CD markers (Fig. 5F, S8). These results demonstrated that one of the mechanisms of synergy between muMyc-EC and anti-PD-1 includes a decrease in regulatory T-cells (Tregs). Increased Treg infiltration in the tumor microenvironment (TME) is a known resistance mechanism of immune checkpoint inhibitors in patients⁴⁵. Collectively, these results indicated that epigenomic downregulation of *Myc* in immune-competent mice enhanced the activity of immune checkpoint inhibitors, in part, through downregulation of PD-L1 expression in tumor cells and a decrease in inhibitory Tregs in the TME.

Discussion

We have described a therapeutic strategy for targeted and sustained control of gene expression that leverages natural gene control mechanisms via precise epigenetic modulation of cis-regulatory elements embedded in IGD structures, thus enabling pre-transcriptional gene control. This approach enables targeted control of genes within dysregulated IGDs that drive numerous processes and states associated with a broad range of human diseases. Importantly, this strategy offers a promising avenue for so-called undruggable targets that are challenging to address with conventional therapeutic interventions, such as small molecules or antibodies. Chromatin-based sequence elements within IGDs represent many potential regulatory intervention points, capable of impacting gene expression in an additive, synergistic, or non-linear manner to precisely and controllably tune the expression of one or multiple genes within an IGD. This approach may be particularly attractive for modulating gene expression in disease states that require restoration of homeostatic levels of gene expression rather than inducing supra- or super-physiological levels as seen with modalities such as small interfering RNAs (siRNA)⁴⁶ or adenoviral mRNA delivery⁴⁷, respectively.

As noted, one promising application of our platform is the potential to selectively control expression of so-called undruggable targets. To assess this, we focused on the *MYC* oncogene, which is an ideal target for evaluation given its well-established role in cancer and the known challenges associated with development of previous *MYC*-targeted therapies. Our approach of targeted *MYC* downregulation through precise and sustained pre-transcriptional

epigenetic modification of *MYC* regulatory elements using a single bicistronic mRNA distinguishes itself from other *MYC*-targeting strategies. For example, multiple approaches have attempted to directly inhibit *MYC* transcript or protein such as antisense oligonucleotides, siRNAs, protein degraders (PROTACs), and polypeptides that block heterodimerization of *MYC* with MAX/MIN that are required for *MYC* activity (e.g., Omo-*MYC*)^{48,49}. However, given that *MYC* mRNA levels are tightly controlled through transcriptional feedback to the *MYC* gene^{4,12}, strategies to directly inhibit *MYC* transcripts or protein are likely to require maintenance of effective drug exposures for sustained periods to offset *MYC* transcriptional upregulation. In contrast, epigenomic controllers are likely to disrupt this autoregulatory transcriptional feedback loop by inducing and maintaining *MYC* transcriptional inhibition. Another approach aimed at inhibiting *MYC* involves transcriptional downregulation through use of small molecules that inhibit general transcriptional machinery (e.g., CDK9-, BET-inhibitors) or that modify DNA secondary structure (e.g., G4-quadruplex stabilizers)^{6,10,50–54}. However, given the lack of specificity with these approaches, undesired off-target effects are likely to limit their utility. Indirect inhibition of *MYC* activity by targeting downstream *MYC* transcriptional targets or synthetic lethal targets, such as BUD, eIF4F, or NUAK1 (ARK5) have also been described^{10,55–57}. However, such approaches are susceptible to activation bypass mechanisms and circumvention of inhibitory activity in *MYC*-dependent cancers. Finally, our approach is also differentiated from other strategies aimed at modifying the epigenomic state of the *MYC* locus through use of CRISPR/dCas tools^{17,18}. Specifically, while CRISPR/dCas utilizes guide RNAs, our approach uses expression of ZF DNA binding domains to precisely target sites within the *MYC* regulatory region. Therefore, precise targeting of different effector activities to different regulatory sites can be achieved based on the combinations of ZF-effector fusions expressed. Moreover, because ZF DNA binding domains have intrinsic DNA binding activity, they are independently active and do not require guide RNAs to be provided as separate components. Due to the small size of the ZF DNA binding domains of MYC-EC-E1 and MYC-EC-E2, the entire OTX-2002-DS mRNA is only ~3.5 kb. Consequently, our approach represents a single, independent drug substance that can readily be packaged in LNPs for systemic in vivo delivery with potential to differentially regulate the epigenetic state of multiple independent sites to maximize the desired targeted effect.

In this study focused on preclinical models of HCC, we evaluated the impact of the *MYC*-targeting epigenomic controller, OTX-2002, illustrating key features of this mRNA therapeutic. First, transfection of single bicistronic OTX-2002-DS mRNA to HCC cells led to translation of both epigenomic controller elements and robust downregulation of *MYC* mRNA and *MYC* protein within 6 h of treatment, associated with the expected site-specific CpG- and H3K9Me3-methylation epigenomic marks in the *MYC* IGD. Second, *MYC* IGD methylation, *MYC* mRNA, and *MYC* protein changes were sustained after clearance of the translated epigenomic controller elements, with evidence supporting partial maintenance of response for up to 15 days after a single dose of treatment. Together, these results support a model in which expression of OTX-2002 epigenomic controller elements leads to rapid and durable changes in the epigenomic state of the *MYC* IGD and consequent swift and enduring changes in *MYC* gene expression. These

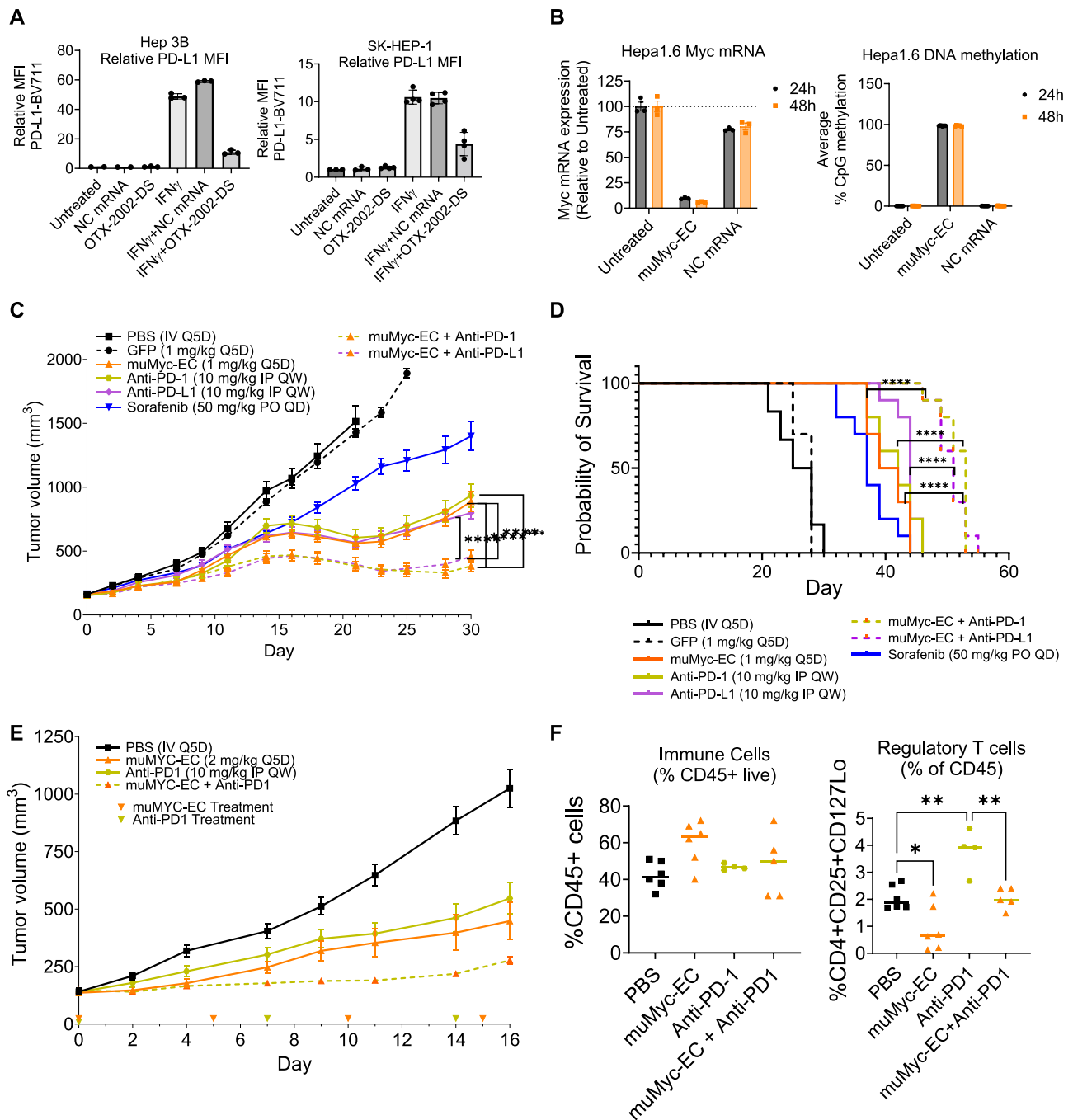


Fig. 5 | OTX-2002 improves efficacy of Anti-PD1 / PD-L1 therapy. **A** MFI calculation (gating strategy Fig S7A, B) using fluorophore conjugated anti-PD-L1 antibody in treated Hep 3B (left) or SK-HEP-1 (right) cells. Results are from one independent experiment (Hep 3B, $n = 2$ technical replicates for untreated and NC mRNA, $n = 3$ technical replicates for all other groups; SK-HEP-1, $n = 3$ technical replicates for untreated and NC mRNA, $n = 4$ technical replicates for all other groups) and were repeated once. **B** Evaluation of Myc mRNA (left) and Myc promoter methylation (right) using murine muMyc-EC in the Hepa1.6 cell line. Results are from one independent experiment (Myc mRNA expression, $n = 3$ technical replicates for all treatments; Myc promoter methylation at 24 h, $n = 9$ technical replicates for all groups, at 48 h, $n = 5$ technical replicates for muMyc-EC, $n = 8$ technical replicates for NC mRNA) and were repeated once. **C** In vivo evaluation of single agents and combinations in Hepa1.6 tumors grown in normal mice. Significance measured using two-way ANOVA comparing muMyc-EC, Anti-PD-1, or Anti-PD-L1 single agents to combinations with adjusted p -values for multiple comparisons; *** $P = 0.0002$ and **** $P < 0.0001$. Results are from one independent

experiment ($n = 12$ mice for PBS group, $n = 10$ mice for all other groups) and were repeated once. **D** Survival curves for combination study in (C) with mice removed at >2000 mm³. Significance was measured using Log-rank (Mantel-Cox) test comparing muMyc-EC, Anti-PD-1, or Anti-PD-L1 single agents to combinations (**** $P < 0.0001$). **E** Hepa1.6 treated tumors collected on Day 16 for TIL analysis. Results (E, F) are from one independent experiment ($n = 14$ mice per group) and were repeated once. **F** Measurement of TILs using flow cytometry (gating strategy Fig. S8). Percentage of immune cells (left) or regulatory T-cells (right) in treated tumors. Results are from one independent experiment ($n = 6$ tumors for PBS, $n = 6$ tumors for muMyc-EC, $n = 4$ tumors for Anti-PD-1, $n = 5$ tumors for muMyc-EC+Anti-PD-1) and were repeated once. Significance measured using one-way ANOVA with adjusted p -values; PBS vs. muMyc-EC * $P = 0.0348$, PBS vs. Anti-PD-1 ** $P = 0.0035$, and Anti-PD-1 vs. muMyc-EC + Anti-PD-1 ** $P = 0.0042$. For all relevant panels error bars represent mean (\pm) standard error of the mean (SEM). Source data are provided as a Source Data file.

kinetics suggest that OTX-2002 may be systemically administered on an intermittent basis while maintaining the desired biological effects between doses, an important clinical consideration for an LNP-encapsulated mRNA-based therapeutic administered intravenously where tolerability is largely based on amount and frequency of LNP delivery⁵⁸.

OTX-2002-DS mediated downregulation of *MYC* RNA and MYC protein resulted in marked reduction in HCC cell viability, with effects observed as early as 24 h post-treatment and reaching near complete loss of viability within 48 to 72 h. Loss of cell viability was associated with increased apoptosis as observed in HCC cell lines representing S1 and S2 HCC subtypes. In vivo, OTX-2002 also resulted in dose-dependent tumor growth inhibition across subtypes, which was associated with a dose-dependent increase in apoptosis and a dose-dependent decrease in proliferation. OTX-2002 was well tolerated in mice at the efficacious doses tested, as demonstrated by minimal BW change and animal survival. Specific analyses of effects on liver function or other tissues were not evaluated in this study since mice are not considered a suitable model for nonclinical toxicology evaluations in vivo⁵⁸. However, the safety and tolerability of OTX-2002 is currently being evaluated in patients with solid tumors, including HCC patients (NCT05497453), and results will be reported in due course.

Our results support the potential for epigenomic downregulation of *MYC* as a strategy to induce or enhance immune-mediated antitumor activity as a monotherapy or in combination with immune checkpoint inhibitors of the PD-L1/PD-1 axis. OTX-2002-DS downregulated PD-L1 in human HCC tumor cell lines, and downregulation of *Myc* in immune-competent mice using a surrogate epigenomic controller element was associated with significant antitumor activity in a syngeneic mouse model of HCC as a monotherapy, which was significantly enhanced in combination with anti-PD-L1 and anti-PD-1 antibodies. Additionally, we found a reduction of Tregs in the TME in the mice treated with the muMyc-EC plus anti-PD-1 combination. Treg infiltration with anti-PD-1 treatment is a known mechanism of resistance to checkpoint inhibitors^{45,59}. While the mechanistic basis for this observation requires further investigation, *Myc* depletion has been shown to reverse immune evasion in preclinical models of lung cancer by modulating the tumor immune phenotype from a T-cell exhaustion state towards memory and effector T-cell phenotypes⁶⁰. Additional studies will help further elucidate the mechanisms by which OTX-2002 exploits the immune system to induce antitumor activity alone and in combination with immune checkpoint inhibitors in preclinical models of HCC.

Further, OTX-2002 significantly enhanced the activities of the tyrosine kinase inhibitors (TKIs) sorafenib³¹ and lenvatinib³², SoC therapies in HCC, which inhibit multiple kinases that drive proliferation and survival of multiple cell types including tumor, vascular, and stromal cells. Our in vitro studies suggest that the enhanced in vivo activity of OTX-2002 combined with either TKI is due, in part, to additive or synergistic activity in HCC tumor cells possibly through enhanced reduction of MYC. However, given that MYC plays a critical role in regulating the tumor microenvironment, including regulation of vascular and stromal cells, future research will help elucidate whether OTX-2002 also enhances TKI activity in these other cell types critical for tumor maintenance.

Since overexpression of MYC has been implicated as a mechanism of TKI resistance with HCC SoCs, clinical exploration of combination therapy with a MYC repressor such as OTX-2002 would be beneficial³⁵. Our findings that the rationale-driven TKI and checkpoint inhibitor combinations are effective both in vitro and in vivo suggest an opportunity to reduce side effects of SoCs while maintaining or improving response by lowering the dose or regimen in the clinic when administered in combination with OTX-2002. The TKI and OTX-2002 combination treatment may also be a way to re-sensitize refractory or resistant tumors.

HCC represents an attractive and clinically tractable indication for development of MYC-targeted mRNA-based therapeutics since MYC has been implicated in development of HCC⁶¹ and systemic delivery of mRNA requires encapsulation in LNPs, which can target liver tissue with high efficiency using current technological approaches^{62,63}. Targeted tissue delivery is desirable when considering modulation of cancer targets since most genes that drive cancer have important functions in normal cells and tissues, and untargeted therapeutics may result in undesired toxicities, which often limit the therapeutic window for maximal clinical benefit in cancer patients. This may be particularly true for pleotropic (TFs) such as MYC that have important functions in multiple tissues. However, it is interesting to note that for MYC itself, systemic inhibition leads to sustained regression of established tumors in preclinical models, with modest and reversible impacts on normal tissues^{10,64}. Consistent with this, our results demonstrated that OTX-2002-DS-mediated downregulation of MYC selectively inhibited viability of HCC tumor cells relative to normal primary hepatocytes in vitro. Also of note, our preclinical data demonstrated antitumor activity in HCC xenografts grown both orthotopically and subcutaneously, indicating that HCC tumor cells established within and outside of the liver retain capacity for targeting with LNPs, suggesting that LNP delivery holds promise for treatment of primary HCC and metastatic disease. Although comprehensive analysis of all organs and tissues targeted by our clinical LNP was not performed in our studies and therefore targeting of non-specific tissues cannot be ruled out, targeted downregulation of MYC through LNP-mediated delivery of specific epigenomic controllers such as OTX-2002 may provide a desirable therapeutic window for effective treatment of primary and metastatic tumors in patients with HCC.

As a programmable mRNA therapeutic designed to controllably downregulate MYC expression pre-transcriptionally through epigenetic modulation, OTX-2002 may be offered as a therapeutic option to patients with HCC. OTX-2002 could find application as a therapeutic for other MYC-dependent tumors in a disease agnostic manner and the epigenomic controller platform technology can be engineered to have similar application across a diverse range of targets, tissues, and indications. These data provide robust preclinical proof of concept and support the rationale for clinical development of OTX-2002 either as a monotherapy or in combination with TKI or immune checkpoint inhibitors in HCC, which is currently under evaluation in an ongoing Phase 1/2 clinical trial (NCT05497453).

Methods

The protocols used for animal studies were reviewed and received ethical approval from the Pharma Models (Marlborough, MA) IACUC and an attending veterinarian at the facility, as necessary, and all animal welfare concerns were addressed and documented. All protocols complied with all institutional tumor policy guidelines. The maximal tumor burden set by the IACUC was 2000 mm³ and was not exceeded in these studies. Sex was not considered for the study design as only female mice were used. Female mice were used for housing purposes. Therefore, disaggregated sex information was not necessary.

Epigenomic controller design and construction

DNA sequences encoding DNA binding proteins targeting 21 bp segments were designed with appropriate linkers and nuclear localization signal sequences in the modular approach discussed elsewhere (in preparation). These sequences were synthesized commercially (ATUM) and cloned into a plasmid containing a T7 polymerase site, a 5' UTR, a Kozak sequence, a 3' UTR, and a synthetic polyA tail. Plasmids were scaled up and linearized using BbsI (New England Biolabs) and mRNA was transcribed and capped using commercially available reagents (New England Biolabs, TriLink, etc). The amino acid sequences of the fusion proteins and the nucleic acid sequences (OTX-2002

mRNA included in Supplementary Information) encoding them are described in International Patent Publication No. WO2022132195.

Cell culture

HCC lines Hep G2 (#HB-8065TM), Hep 3B (#HB-8064TM) SK-HEP-1 (#HTB-52TM), SNU-182 (#CRL-2235TM), Hepa1-6 (#CRL-1830TM) were purchased from ATCC® and cultured according to vendor recommendations. PHH were purchased from Lonza (#HUCPG, lot #HUM200271) and cultured according to vendor recommendations. The human cell lines are male and mouse cell line is female.

In vivo formulation

In vivo LNP formulations for EC testing in human xenografts were prepared by Acuitas Therapeutics as described previously⁶⁵. Briefly, the mRNA in acidic aqueous solution was rapidly mixed with an ethanolic solution of cholesterol, 1,2-distearoyl-sn-glycero-3-phosphocholine, a polyethylene glycol lipid, and an ionizable lipid (pKa in the range of 6.0–6.5). The proprietary polyethylene glycol lipid is described in International Patent Publication No. WO 2015/199952A1, and the proprietary ionizable lipid and the LNP composition are described in International Patent Publication No. WO 2017/075531A1⁶⁶. The average particle size, measured by dynamic light scattering, was 53 nm with a polydispersity index of 0.08 and an encapsulation efficiency of 98%. Acuitas will formulate mRNA in the LNP used in this work to academic investigators upon request.

LNP formulations for EC testing in mouse xenografts were produced via microfluidic mixing of an aqueous phase containing the mRNA and an ethanol phase containing lipids. The ethanol phase contained a cationic lipid (MC3) mixed with cholesterol, 1,2-distearoyl-sn-glycero-3-phosphocholine, and 1,2-dimyristoyl-rac-glycero-3-methoxypolyethylene glycol-2000. The average particle size, measured by dynamic light scattering, was 104 nm with a polydispersity index of 0.05 and an encapsulation efficiency of 96%.

Formulation preparation for in vitro use

LNPs were formulated using the NanoAssemblr® SparkTM (#NIS0003, Precision Nanosystems) prior to transfection and stored on ice or 4 °C until use. RNA mix for each OEC was diluted in malic acid buffer and loaded into Spark Cartridges (#NIS0009, Precision Nanosystems) along with PBS (# 21-040-CV, Corning) and research lipid. The loaded Spark Cartridge was then installed into the NanoAssemblr® SparkTM for final LNP assembly.

Transfections

HCC cells were trypsinized and seeded into flat bottomed 96-well microplates (#3628, Corning) at a density of 10,000 cells/well. Prepared LNP formulations were diluted into growth media and added to the plated cell suspension to achieve desired final LNP concentration. Plates were incubated for desired time point and cells were lysed for subsequent analysis (RT-qPCR, Cell viability, Methylation analysis, etc). All treatments were performed in biological triplicates. PHH cells were transfected with LNP for 6 h with partial media changes then complete media change every 24 h thereafter until collection. Transfection efficiency was calculated using the CellTiter-Fluor cell viability assay (Promega) and ONE-Glo luciferase assay system (Promega) according to the manufacturer's protocol 24 h post transfection with firefly luciferase.

Real-time quantitative polymerase chain reaction (RT-qPCR)

RNA was isolated from three technical replicates, using the RNeasy plus 96-well Kit (Qiagen) following the manufacturer's protocol. RNA samples were retrotranscribed to cDNA using LunaScript RT Super-Mix Kit (New England Biolabs) and analyzed by quantitative PCR (qPCR) (in technical triplicates) using a MYC-specific Taqman primer/probe set assay (Hs00905030_m1, FAM, ThermoFisher Scientific)

with the Taqman Fast Advanced Master Mix (ThermoFisher Scientific). MYC expression was quantified relative to the expression of GAPDH reference genes (Hs99999905_m1, VIC, ThermoFisher Scientific) and reported as fold change using the following formula; $2^{-\Delta\Delta Ct}$ where the delta delta Ct ($\Delta\Delta Ct$) method; $\Delta\Delta Ct = \Delta Ct(a \text{ treated sample}) - \Delta Ct(a \text{ control sample})$, $\Delta Ct(a \text{ treated sample}) = (Ct \text{ of MYC in treated sample} - Ct \text{ of GAPDH in treated samples})$, $\Delta Ct(a \text{ control sample}) = (Ct \text{ of MYC in control sample}) - Ct \text{ of GAPDH in control samples}$.

Cell viability analysis

Viability was measured using the CellTiter-Glo assay kit (Promega) according to manufacturer's protocol. Cellular apoptosis was measured by either using the Annexin V antibody to bind apoptotic cells and quantified via flow cytometry, or the RealTime-Glo Annexin V Apoptosis and Necrosis kit (Promega) according to the manufacturer's protocol.

Antibodies for immunohistochemistry (IHC) staining, western blotting, and flow cytometry

Western blotting (1:1000 dilution of all primary antibodies listed in 10 mL of Intercept® T20 (TBS) Antibody Diluent, LI-COR) and IHC (1:200 dilution of all primary antibodies listed in 10 mL buffer containing 3% serum blocking solution): Caspase-3 antibody (ab184787, clone EPR18297, Abcam), anti-Ki67 antibody (ab197547, clone SP6, Abcam), anti-AFP antibody (ab169552, clone EPR9309, Abcam), anti-MYC antibody (ab32072, clone Y69, Abcam), anti-HA antibody (ab18181, clone HA.C5, Abcam). In vitro PD-L1 surface expression (1:200 dilution of all primary antibodies listed in 100 μ L of InvitrogenTM eBioscienceTM Flow Cytometry Staining Buffer): Anti-Human PD-L1 antibody (BV711; Biolegend 329722, clone: 29E.2A3). Immune cell profiling from fresh tumors using flow cytometry (1:200 dilution of all primary antibodies listed in 100 μ L of InvitrogenTM eBioscienceTM Flow Cytometry Staining Buffer): APC/CY7- CD45.2 (Clone 104, Biolegend 109824), BV421- CD3E (Clone 145-2C11, Biolegend 100335), FITC-CD4 (Clone RM4-5, Biolegend 100509), Alexa Fluor647- CD25 (Clone PC61, Biolegend 102020), BV605- CD127 (Clone A7R34, Biolegend 135041).

Immunoblot protocol

Culture media was aspirated from cells and 60–80 μ L of radio-immunoprecipitation assay buffer containing protease inhibitors was added to each well and the cells were dissociated using a cell scraper. Lysate was transferred to an Eppendorf tube. The lysate was incubated on ice for 30 min then spun in a microcentrifuge at top speed for 20 min. The supernatant was transferred to a new Eppendorf tube and quantified using the BCA Protein Assay (ThermoFisher Scientific) using the 96-well format according to manufacturer's recommendations. About 10–50 μ g of total protein was used to load into each well of a denaturing SDS-PAGE gel. Briefly, denatured protein lysate was generated using 5 μ L Invitrogen NuPage Gel Loading Buffer (ThermoFisher Scientific), 2 μ L Invitrogen NuPage Sample Reducing Agent (ThermoFisher Scientific) and up to 17 μ L of protein lysate (plus water if needed) to bring the volume to 20 μ L then boiled at 90 °C for 10 min. The denatured lysate was run in a 4–12% Invitrogen Bis-Tris gel (ThermoFisher Scientific) with 1x MOPS buffer. Chameleon protein ladder (LI-COR Biosciences) was used to determine the size of the proteins after separation. The gel was transferred according to iblot2 protocol (ThermoFisher Scientific) onto PVDF membrane (ThermoFisher Scientific). Once transferred, the PVDF membrane was placed into LI-COR Biosciences' blocking reagent for 60 min then put into 10 mL of intercept antibody diluent with appropriate antibodies. The membrane was incubated in primary antibody overnight at 4 °C. The next day the membrane was washed then incubated with the appropriate secondary antibody (typically a red and green LI-COR secondary antibody for mouse and rabbit at 1:5000 in 10 mL of Intercept® T20

(TBS) Antibody Diluent, LI-COR) for 1 h at room temperature. The membrane was washed then imaged on LI-COR Odyssey Imaging System to obtain fluorescent signal on the 700 and 800 channels, which correlate to the secondary antibodies. The LI-COR Image Studio software was used to obtain quantification of fluorescent signal for each band present on the blot.

IHC staining of tumor samples

Slides were prepared from mouse xenograft formalin-fixed, paraffin-embedded blocks and were baked in a 60 °C oven for 1 h and deparaffinized by immersing them into xylene twice for 5 min. The slides were then rehydrated through sequential immersion in 100%, 95%, 80% ethanol, and distilled water (dH₂O) for 5 min each. The slides were then immersed in EDTA solution (pH.9.0) for 15 min at 95 °C for antigen retrieval. After antigen retrieval, the slides were washed with dH₂O for 5 min, and then blocked with BLOXALL (#SP-6000, Vector Labs) for 20 min at room temperature. Slides were washed twice with PBST (1XPBS with 0.05% Tween-20) washing buffer. The slides were further blocked with serum free blocking solution (#ab64226, Abcam) before incubating with the appropriate antibody at 1:200 dilution in 10 mL diluent containing 3% serum blocking solution at 30 °C for 1 h. After antibody incubation, the slides were washed with PBST washing buffer and incubated with ready to use Rabbit Specific HRP/DAB Micro-polymer detection kit (#ab236469, Abcam). The color development of primary antibody signal was achieved by incubating slides in DAB solution for 5 min at room temperature. The resulting brown color staining represents primary antibody positive cells. The slides were then washed twice with dH₂O and then counter stained with hematoxylin for nuclei counter staining. The slides were then dehydrated through 100% ethanol treatment followed by final immersion in xylene. The slides were mounted with xylene based mounting media (#s2153-8oz, Poly Scientific R&D Corp.) and then air dried. All IHC slides were imaged at 10× and 20× using a bright field Olympus BX53 microscope (Leica Biosystems) equipped with a DP74 digital camera.

IHC quantification

The image files were exported to QuPath⁶⁷ for analysis and processing. The “Cell detection” feature was employed with default settings maintained, except for an adjustment to the requested pixel size to align with the original microscope settings. The color deconvolution staining estimate was set to “H-DAB”. Cells positive for individual marker Ki67, Caspase-3, MYC, and AFP were identified based on the DAB optical density, with a threshold used to distinguish between positive and negative cells. The number of marker-positive cells for each stain was normalized to the total number of cells per field (3 fields counted per image), yielding a percentage of IHC-positive cells for each field. These percentages were subsequently averaged across all fields for each sample to provide an overall expression index for each xenograft tumor. The analyzed data were then exported to an Excel file for further analysis and graphing.

Annexin V apoptosis

Hep 3B, Hep G2, or SK-HEP-1 cells were plated in 12-well plates at 100,000 cells per well culture media. The plates were treated in quadruplicate with OTX-2002 and a negative control test compound at 1 µg/mL for cell viability analysis. Cells were incubated for 48 h, with a subset of cells at each timepoint left as untreated as an additional negative control. Following their incubation period, the plates were briefly spun to collect dead and live cells. Cells were dissociated from their wells and transferred to a round bottom 96-well plate. Following a PBS wash, cells were stained with PI and Annexin-V FITC for apoptosis analysis. Samples were then analyzed through flow cytometry (Cytek Aurora), where cells positive for both conjugates indicate induction of apoptosis following treatment.

PD-L1 cell surface expression

Cells were treated in duplicate for surface PD-L1 expression analysis. Cells were exposed to treatment continuously for 48 h with OTX-2002 or negative control (NC) mRNA at 1 µg/mL or left untreated. Following 24 h of incubation period with OTX-2002 or NC mRNA treatment, cells were stimulated with human IFN-γ at 50 ng/ml. Following 24-h stimulation with IFN-γ (total 48 h incubation with OTX-2002 or NC mRNA), cells in one plate were harvested for flow cytometry. Cells were washed with HBSS buffer and removed from the plate using TrypLE for 5 min. Afterwards cells are washed with PBS and spun. Cells were stained for 30 min in 50 µl volume with desired dilution of antibody and live/dead aqua stain (PD-L1 BV711 antibody 1:200 dilution in 100 µl of Invitrogen™ eBioscience™ Flow Cytometry Staining Buffer). Cells were washed with FACS or PBS buffer, resuspended in FACS buffer in the plate, and analyzed by flow cytometer (Cytek Aurora).

Targeted DNA methylation assessment

Cells were disassociated, collected, and lysed according to the MasterPure Purification kit (Lucigen). Cells were lysed in a solution containing proteinase K. Lysate was incubated at 65 °C and then cooled to 37 °C. Lysate was then treated with RNaseA and proteins were precipitated using Lucigen MPS protein precipitation reagent. Precipitate was pelleted and supernatant harvested for DNA purification. DNA was precipitated from the sample using isopropanol, washed and resuspended in Tris-EDTA buffer (TE). Purified DNA was then utilized for methylation analysis using amplicon methylation sequencing. gDNA was sheared to -15 kb fragments on a PIXUL acoustic Sonicator (Active Motif) and then subjected to an enzymatic conversion reaction (NEBNext Enzymatic Methyl-seq [EM-seq™] (New England Biolabs) that converts unmethylated cytosines to uracils while leaving methylated cytosines unaffected. The MYC promoter was PCR-amplified from converted, deaminated gDNA using a uracil-competent polymerase, Q5U (New England Biolabs) with target specific primers, and Next Generation Sequencing libraries were prepared from the product for Illumina sequencing to evaluate methylation at base-pair resolution. The sequencing reads were trimmed, and Bismark (Houda A. Belaghal, Jeremiah D. Farelli, Thomas G. McCauley, Charles W. O'Donnell, manuscript under consideration) was used for reads alignment and quantification. The methylation values were estimated based on the methylated ratio on individual cytosine-guanine dinucleotide (CpG), or CHG, and CHH (where H correspond to A, T or C) sites. Differentially methylated regions were identified by DMRSeq (William Senapedis, Elmer Figueroa, Kayleigh Gallagher, Jeremiah Farelli, Robert Lyng, Charles O'Donnell, Joseph Newman, Thomas McCauley; Abstract 2629, Cancer Res 15 June 2022; 82 (12 Supplement): 2629), and differentially methylated CpG sites were identified by using Limma¹⁹.

RNA sequencing analysis

RNA was isolated using the RNeasy mini kit (Cat. #74106, Qiagen) on Qiacubes with QC and quantification using the TapeStation (Agilent Technologies) and Qubit 2.0 Fluorometer (ThermoFisher Scientific). RNA sequencing libraries were prepared using the NEBNext Ultra II RNA Library Prep Kit for Illumina using manufacturer's instructions (New England Biolabs). Briefly, mRNAs were enriched with Oligod(T) beads and fragmented for 15 min at 94 °C. After first and second strand cDNA synthesis, cDNA fragments were end repaired and adenylated at 3'ends. Universal adapters were ligated to cDNA fragments, followed by index addition and library enrichment by PCR with limited cycles. Sequencing libraries were validated on the TapeStation (Agilent Technologies), and quantified by using Qubit 2.0 Fluorometer (ThermoFisher Scientific) as well as by quantitative PCR (KAPA Biosystems). The sequencing libraries were multiplexed and sequenced on an Illumina HiSeq using a 2 × 150 bp Paired End (PE) configuration.

Bioinformatic analysis

Illumina sequencing data in FASTQ format was collected and QCed using FASTQC, and reads were trimmed using Trimmomatic to remove sequencing adaptors. Transcripts were quantified at transcript level using Salmon with hg19 index files created from ensembl transcript files⁶⁸. Quantification of transcripts from Salmon were aggregated to gene level expression using tximport. Differential expression and pathway enrichment analyses were performed using R (version 4.3). DESeq2 (version 1.41.2) was used to estimate variance-mean dependence in read count table and test for differential expression of genes between OEC treatments and control groups based on negative binomial distribution. The Wald test was used in DESeq2 for statistical significance testing and generating *p* values for differential analysis, with adjustment for multiple testing (Benjamini and Hochberg). Log2FC and adjusted *p* value were used as thresholds to filter and subset genes that have significantly differential gene expressions due to treatments. Both Spearman correlation and Pearson correlation analysis were performed to ensure the correlations between replicates and groups. High-dimensional transcriptomic space was projected to lower dimension using PC1 and PC2 from principal component analysis to visualize the distribution of samples. A Volcano plot was created to visualize the global distribution of differential gene expressions using log2FC and $-\log_{10}(\text{adj.}P \text{ value})$ as two-dimensional features.

Gene set enrichment analysis

A sorted, unfiltered list of *t*-statistics for each gene from the differential analysis was used as input to fGSEA (v1.25.2) with the HALLMARK gene set from MSigDB (<https://www.gsea-msigdb.org/>). fGSEA calculates an enrichment score for the input list and estimates *p* values for each gene set based on the probability of observing an equal or greater enrichment score across 1000 permutations of the input gene list, divided by the total number of permutations. Once more, the BH method was used to calculate FDR for the resulting *p* values to account for multiple testing, and an adjusted *p* value of <0.05 was considered significant.

Chromatin immunoprecipitation quantitative polymerase chain reaction (ChIP-qPCR)

Crosslinked cells were thawed and resuspended in a lysis buffer suitable for the isolation of nuclei. The isolated nuclei were then sonicated to yield sheared DNA of between 200 and 700 bp. Isolated sheared chromatin was then used for input preparation and ChIP. For input, 10% of isolated sheared chromatin was removed and treated with RNase A, proteinase K, and heated to degrade RNA and proteins. The input DNA was purified using MinElute Reaction Cleanup Kit (Cat # 28206, Qiagen). The remaining sheared chromatin was used for H3K9me3-ChIP with the ChIP-IT High Sensitivity Kit (Cat. #53040, Active Motif). Briefly, sheared chromatin, 1.5 μg anti-H3K9me3 antibody (Cat. #ab176916, Abcam), protease inhibitors and ChIP buffer were mixed and incubated overnight at 4 °C. During this time, protein G agarose beads were washed and prepared. After the overnight incubation, the protein G agarose beads were added to the chromatin:antibody mixture and incubated for another 3 h at 4 °C. After incubation, the mixture was added to a filter column, washed several times with wash buffer, and then the antibody:bound chromatin mixture was eluted from the beads using an elution buffer. Chromatin was reverse crosslinked using proteinase K and incubated at 55 °C for 30 min and then 65 °C overnight. ChIP DNA was purified using MinElute Reaction Cleanup Kit (Cat. #28206, Qiagen). Quantitative PCR (qPCR) reactions were carried out in triplicate on specific genomic regions using SYBR Green Supermix (Cat # 170-8882, Bio-Rad) on a QuantStudio™ 7 Pro real-time PCR system (Thermo Fisher Scientific). Primers used Forward: CTTTACTTTTCGAAACCTGAAC, Reverse: GGGAGCAACCAATCGCTATG). The percent input method was used to determine factor enrichment. The starting input fraction was 10%, therefore a dilution factor of 10 or 3.321 cycles (i.e., log₂ of 10) was subtracted

from the Ct value of diluted input to adjust input to 100%. Percent input was calculated according to the formula: $100 \times 2^{(\text{Adjusted input Ct} - \text{Ct (IP)})}$.

Laboratory animals used in this manuscript

Human HCC was induced in female nude (outbred athymic NU/J; #007850; *Foxn1^{tm1}/Foxn1^{tm1}*) mice (*Mus musculus*; age 5–6 weeks). Hepa1.6 (mouse liver cancer cell line) subcutaneous syngeneic model was implanted in female C57BL/6 normal (Jackson Labs inbred B6; strain #000664) mice (*Mus musculus*; age 8 weeks). Animals were housed in small groups of ~5 animals per cage. AlphaDri® bedding was used. Bedding was changed a minimum of once per week. Animals were acclimatized prior to study commencement. During this period, the animals were observed daily in order to reject animals that were present in poor condition. The studies were performed in animal rooms provided with filtered air at a temperature of 70 ± 5 °F and $50\% \pm 20\%$ relative humidity. Animal rooms were set to maintain a minimum of 12–15 air changes per hour. The room was on an automatic timer for a light/dark cycle of 12 h on and 12 h off with no twilight. The temperature and relative humidity were recorded during the study, and the records retained. Animals were fed with Envigo 2920X or equivalent sterile rodent chow and sterile water provided ad libitum.

Subcutaneous HCC xenograft tumor models

Human HCC (Hep 3B, Hep G2 and SK-HEP-1) was induced in female nude (outbred athymic NU/J; #007850; *Foxn1^{tm1}/Foxn1^{tm1}*) mice (*Mus musculus*; age 5–6 weeks), which were inoculated subcutaneously in the left flank with 1×10^7 HCC cells. Treatment was initiated when the tumors reached a mean volume of 150 mm³. Mice were allocated into groups (*n* = 10 mice per group) such that mean tumor volume in each group was within similar range. Mice were treated with PBS, OTX-2002 (3, 1, 0.3 mg/kg) or negative control (NC) mRNA given via intravenous injection (IV) once every five days (Q5D). Sorafenib (50 mg/kg) was given via oral gavage (PO) once a day (QD). Animal weights and conditions were recorded daily. Tumors were measured on Mondays, Wednesdays, and Fridays by measuring each tumor in two dimensions, first by measuring the longest dimension (length or *L*), and then the dimension perpendicular to this (width or *W*). Tumor volumes were calculated using the standard formula: $(L \times W^2)/2$. The mean tumor volume and standard error of the mean was calculated for each group at each time point.

Subcutaneous HCC xenograft tumor models for luciferase imaging

Hep 3B was induced in female nude (outbred athymic NU/J; strain #007850; *Foxn1^{tm1}/Foxn1^{tm1}*) mice (*Mus musculus*; age 5–6 weeks), which were inoculated subcutaneously in the left flank with 1×10^7 HCC cells. Treatment was initiated when the tumors reached a mean volume of 150 mm³. Mice were treated once with PBS or luciferase mRNA in Acuitas LNP at 3 mg/kg. At 6 h mice were anesthetized and luciferase was imaged by in vivo imaging system (IVIS from Perkin Elmer). The images were used for quantification of tumor and liver signal in the vivo mouse.

Orthotopic Hep 3B xenograft model in nude mice

Female nude (outbred athymic NU/J; strain #007850; *Foxn1^{tm1}/Foxn1^{tm1}*) mice (*Mus musculus*; age 5–6 weeks), (*n* = 10 per group) were orthotopically implanted with 1×10^4 Hep 3B-luciferase cells. Mice were allocated to six groups of ten mice such that mean tumor volume in each group was within the range of 4.7×10^7 to 7.6×10^7 photons/s. Intravenous treatment with OTX-2002 (2, 1 or 0.5 mg/kg Q5D), negative control mRNA formulated in the same LNP (2 mg/kg IV Q5D), or PBS (10 mL/kg IV Q5D) were initiated when the tumors reached a mean luminescence of 5.8×10^7 photons/s (standard deviation $\pm 5.6 \times 10^7$ photons/s,

CV = 96.3%, range 4.7×10^6 – 2.0×10^8 photons/s). In vivo studies conducted per external research organizations IACUC Policy.

In vitro combination therapy of OTX-2002-DS with tyrosine kinases in HCC

HCC cells were maintained in EMEM media with fetal bovine serum in a tissue culture incubator at 37 °C, 5% CO₂. When cells reached 80% confluency, they were passaged at a 1:3 ratio. OTX-2002 DS was formulated in the SSOP LNP. Hep 3B or SK-HEP-1 cells were plated in 96 well plates at 10,000 cells per well in EMEM media. Cells were then treated with lenvatinib or sorafenib. The dose range for lenvatinib was between 0.004 and 25 μM, with each dose being serially diluted 1:3 or 1:2, respectively. LNP mix carrying OTX-2002 DS was added to a subset of the wells at a dose of 0.06 μg/mL, 0.6 μg/mL, or 1.0 μg/mL. A subset of cells was left untreated to determine the effect of lenvatinib or sorafenib alone. Cells were incubated for 72 h. Following treatment, cell viability was analyzed using Cell Titer Glo (Promega). Relative cell viability was calculated by averaging the untreated values and dividing each experimental luciferase value by that average.

Synergy calculations

Bliss synergy scores (Table 1 and Fig. S6A) were calculated using SynergyFinder 2.0 to determine combinatorial effect⁶⁹. The degree of combination synergy, or antagonism, was quantified by comparing the observed drug combination response against the expected response, calculated using a reference model that assumes no interaction between drugs. The Bliss independence model assumes a stochastic process in which two drugs elicit their effects independently, and the expected combination effect can be calculated based on the probability of independent events. In general, if the synergy score was <−10 the interaction between two drugs was likely to be antagonistic; scores between −10 and 10 suggest the interaction between two drugs was likely to be additive; at scores >10 the interaction between two drugs was likely to be synergistic.

In vivo combination therapy of OTX-2002 with tyrosine kinases in Hep 3B subcutaneous models

After establishing Hep 3B subcutaneous model in female nude (outbred athymic NUJ); strain #007850; *Foxn1^{tmw}/Foxn1^{tmw}* mice (*Mus musculus*; age 5–6 weeks), treatment was initiated when the tumors reached a mean volume of 150 mm³. Mice were allocated to six groups of eight (lenvatinib) or ten (sorafenib) mice such that mean tumor volume in each group was about 150 mm³. Mice were treated with PBS (IV Q5D), negative control mRNA (0.3 mg/kg or 1 mg/kg IV Q5D), OTX-2002 (0.3 mg/kg or 1 mg/kg IV Q5D), sorafenib (25 mg/kg PO QD), lenvatinib (15 mg/kg QD PO) or combinations of OTX-2002 plus sorafenib or lenvatinib. Animal weights and conditions were recorded daily, and tumors were measured three times a week. In vivo studies conducted per external research organizations IACUC Policy.

In vivo combination therapy of muMyc-EC with immune checkpoint inhibitors in Hepa1.6 subcutaneous models

After establishing Hepa1.6 (mouse liver cancer cell line) subcutaneous syngeneic model in female C57BL/6 normal (Jackson Labs inbred B6; strain #000664) mice (*Mus musculus*; age 8 weeks), treatment was initiated when the tumors reached a mean volume of 150 mm³. Mice were allocated to eight groups of ten mice such that mean tumor volume in each group was about 150 mm³. Mice were treated with PBS (IV Q5D), GFP control mRNA (1 mg/kg IV Q5D), muMyc-EC (1 mg/kg IV Q5D), anti-Pd1 (10 mg/kg intraperitoneal [IP] once per week [QW]; clone RMP1-14, BioXcel Therapeutics), anti-Pd-L1 (10 mg/kg IP QW; clone 10 F.9G2, BioXcel Therapeutics), a combination of muMyc-EC plus anti-PD-1 or anti-PD-L1, or sorafenib (50 mg/kg PO QD). Animal weights and conditions were recorded daily, and tumors were

measured three times a week. In vivo studies conducted per external research organizations IACUC Policy.

In vivo combination therapy of muMyc-EC with anti-Pd-1 in Hepa1.6 subcutaneous models to evaluate tumor infiltrating lymphocytes (TIL)

After establishing Hepa1.6 (mouse liver cancer cell line) subcutaneous syngeneic model in female C57BL/6 normal mice (Jackson Labs inbred B6; #000664) mice (*Mus musculus*; age 8 weeks), treatment was initiated when the tumors reached a mean volume of 150 mm³. Mice were treated with muMyc-EC and Anti-Pd-1 therapies alone and in combination. Sixteen days after initiation of treatment (24 h after last muMyc-EC dose) mice were sacrificed with tumor freshly extracted and preserved on ice. Tumors were weighed and processed using Miltenyi protocol tumor dissociation mouse kit (130-096-730). Following dissociation, cells were moved to a 15 mL conical tube with 70 μm filter attached. The cell chunks were pushed through the filter then washed with 10 ml RPMI media and pelleted at 300 g. Cells were resuspended in an appropriate volume of mouse RBC lysis buffer (Thermo Fisher; J62150.AK) and incubated for 10 min on ice. Cells were resuspended in 100 μL flow cytometry staining buffer (eBioscience) and Fc Block (Miltenyi) for 30 min at 4 °C. The blocked cells were split into separate groups for staining (IgG, unstained, Fluorescence minus one [FMO] and single stain controls) and pelleted in a 96 well plate. Pellets were resuspended in staining mix that included either all antibodies, all antibodies minus one (FMO), single antibody control or IgG control and stain for 1 h. Cells are spun down and resuspended in 150 μL flow staining buffer and transferred to round bottom 96 well plate. The plate was run on Cytek Aurora.

Gating strategy for TIL analysis using Cytek Aurora

Fluorophore compensation was completed using Aurora Cytek unmixing software. Gating of immune cells was performed in FlowJo (Fig. S8). Lymphocytes were distinguished from tumor cells using SSC-A/FSC-A and then characterized into single cells using FSC-H/FSC-A. Immune cells were identified using the CD45 marker. Cells positive for CD45 were then further characterized using CD3 to quantify T cells. T cells were categorized as CD4 or CD8. Activated cytotoxic T cells were defined as cells that were CD8 positive and CD69 positive. Regulatory T cells were defined as cells that were CD4 and CD25 positive as well as negative for CD127.

Statistics and reproducibility

For each tumor growth study, 8–12 tumor-bearing mice were used with specific numbers listed in the method and figure legends. No statistical method was used to predetermine sample size. For each tumor growth study, mice were randomized into control and treatment groups prior to treatment to establish a mean tumor volume of 150 mm³. This number of animals were used to generate sufficient statistical assessment (using one-way or two-way ANOVA) at the end of treatment periods. For each tumor growth study, the study director at the animal facility was blinded to the treatment modality in terms of LNP negative control and active treatment except for PBS negative control and standard of care positive control which were provided by the study director. Results are presented from one independent study. In vivo experiments were independently repeated as noted in the figure legend. In vitro assays were performed in duplicate or more experiments based on historical data. All in vitro experiments were repeated in greater than or equal to two biological replicates with greater than or equal to two technical replicates included. Specific replicates are listed in figure legends. In vitro experiments were not randomized. For in vitro experiments, the investigators were not blinded to allocation during experiments and outcome assessment. For Fig. S2, one of the untreated luciferase values for PHH was negative and cannot be plotted on a log scale. Therefore, this data point was

excluded from the graph with the data available in Source Data File. No *in vivo* data was excluded from the analysis.

Statistics were done using GraphPad Prism (version 10.1.2) algorithms and were one- or two-way ANOVA tests, or Log-rank (Mantel-Cox) test (survival curves) as indicated in individual figure legends. Error bars represent means \pm standard error of the mean as calculated by GraphPad Prism.

Software information

Data was collected and organized with Microsoft® Word, Excel and PowerPoint® for Microsoft Office 365 MSO (Version 2405 Build 16.0.17628.20006) and Graphpad Prism (version 10.1.2), Western blot data was collected on the LI-COR Image Studio software (version 6.0). Flow cytometry data were collected on SpectroFlo (version) then analyzed using FlowJo (version 10.10), RT-qPCR data was collected using QuantStudio™ 7 Pro real-time PCR system Software (Thermo Fisher Scientific). Cell viability and apoptosis was collected using GlowMax Microplate Reader software (version 4.1). QuPath (version 0.5.1) was used for IHC quantification. RNA Sequencing libraries were validated on the TapeStation (Agilent Technologies) and quantified by using Qubit 2.0 Fluorometer (ThermoFisher Scientific) as well as by quantitative PCR (KAPA Biosystems). The sequencing libraries were multiplexed and sequenced on an Illumina HiSeq using a 2 × 150 bp Paired End (PE) configuration. Hallmark gene sets were collected from MSigDB (<https://www.gsea-msigdb.org>) to estimate the transcriptomic enrichment in summarized and well-defined biological states or processes and provide delineated gene space for GSEA.

Reporting summary

Further information on research design is available in the Nature Portfolio Reporting Summary linked to this article.

Data availability

All source data supporting the findings of this study are available within the paper and its Supplementary Information and Source Data file. Individual data points are shown when possible or included in supplementary tables. The RNA-seq data generated in this study have been deposited in the NCBI Sequence Read Archive (SRA) under accession numbers SRR26266137, SRR26266144, SRR26266134, SRR26266139, SRR26266136, SRR26266140, SRR26266141, SRR26266135, SRR26266142, SRR26266133, SRR26266143, SRR26266138 (<https://www.ncbi.nlm.nih.gov/bioproject/PRJNA1023541>). All data is publicly available. Source data are provided with this paper.

References

- Jain, M. et al. Sustained loss of a neoplastic phenotype by brief inactivation of MYC. *Science* **297**, 102–104 (2002).
- Sodir, N. M. et al. MYC instructs and maintains pancreatic adenocarcinoma phenotype. *Cancer Discov.* **10**, 588–607 (2020).
- Soucek, L. et al. Inhibition of MYC family proteins eradicates KRas-driven lung cancer in mice. *Genes Dev.* **27**, 504–513 (2013).
- Dhanasekaran, R. et al. The MYC oncogene—the grand orchestrator of cancer growth and immune evasion. *Nat. Rev. Clin. Oncol.* **19**, 23–36 (2022).
- Felsher, D. W. MYC inactivation elicits oncogene addiction through both tumor cell-intrinsic and host-dependent mechanisms. *Genes Cancer* **1**, 597–604 (2010).
- Dhanasekaran, R. et al. MYC ASO impedes tumorigenesis and elicits oncogene addiction in autochthonous transgenic mouse models of HCC and RCC. *Mol. Ther. Nucleic Acids* **21**, 850–859 (2020).
- Giuriato, S. et al. Sustained regression of tumors upon MYC inactivation requires p53 or thrombospondin-1 to reverse the angiogenic switch. *Proc. Natl. Acad. Sci. USA* **103**, 16266–16271 (2006).
- Soucek, L. et al. Modelling MYC inhibition as a cancer therapy. *Nature* **455**, 679–683 (2008).
- Sodir, N. M. et al. Reversible MYC hypomorphism identifies a key Myc-dependency in early cancer evolution. *Nat. Commun.* **13**, 6782 (2022).
- Llombart, V. & Mansour, M. R. Therapeutic targeting of “undruggable” MYC. *EBioMedicine* **75**, 103756 (2022).
- Wolf, E. & Eilers, M. Targeting MYC proteins for tumor therapy. *Annu. Rev. Cancer Biol.* **4**, 61–75 (2020).
- Dang, C. V. MYC on the path to cancer. *Cell* **149**, 22–35 (2012).
- Hnisz, D., Day, D. S. & Young, R. A. Insulated neighborhoods: structural and functional units of mammalian gene control. *Cell* **167**, 1188–1200 (2016).
- Rao, S. S. et al. A 3D map of the human genome at kilobase resolution reveals principles of chromatin looping. *Cell* **159**, 1665–1680 (2014).
- Feehley, T., O'Donnell, C. W., Mendlein, J., Karande, M. & McCauley, T. Drugging the epigenome in the age of precision medicine. *Clin. Epigenetics* **15**, 6 (2023).
- Bouwman, B. A. & de Laat, W. Getting the genome in shape: the formation of loops, domains and compartments. *Genome Biol.* **16**, 154 (2015).
- Schuijers, J. et al. Transcriptional dysregulation of MYC reveals common enhancer-docking mechanism. *Cell Rep.* **23**, 349–360 (2018).
- Cao, C. et al. A CRISPR/dCasX-mediated transcriptional programming system for inhibiting the progression of bladder cancer cells by repressing c-MYC or activating TP53. *Clin. Transl. Med.* **11**, e537 (2021).
- Lei, Y. et al. Targeted DNA methylation *in vivo* using an engineered dCas9-MQ1 fusion protein. *Nat. Commun.* **8**, 16026 (2017).
- Renbaum, P. et al. Cloning, characterization, and expression in *Escherichia coli* of the gene coding for the CpG DNA methylase from *Spiroplasma* sp. strain MQ1(M.SssI). *Nucleic Acids Res.* **18**, 1145–1152 (1990).
- Stepper, P. et al. Efficient targeted DNA methylation with chimeric dCas9-Dnmt3a-Dnmt3L methyltransferase. *Nucleic Acids Res.* **45**, 1703–1713 (2017).
- Ryan, R. F. et al. KAP-1 corepressor protein interacts and colocalizes with heterochromatic and euchromatic HP1 proteins: a potential role for Kruppel-associated box-zinc finger proteins in heterochromatin-mediated gene silencing. *Mol. Cell Biol.* **19**, 4366–4378 (1999).
- He, T. C. et al. Identification of c-MYC as a target of the APC pathway. *Science* **281**, 1509–1512 (1998).
- Goossens, N., Sun, X. & Hoshida, Y. Molecular classification of hepatocellular carcinoma: potential therapeutic implications. *Hepat. Oncol.* **2**, 371–379 (2015).
- Zhao, Y. et al. RNAi silencing of c-Myc inhibits cell migration, invasion, and proliferation in HepG2 human hepatocellular carcinoma cell line: c-Myc silencing in hepatocellular carcinoma cell. *Cancer Cell Int.* **13**, 23 (2013).
- Whitfield, J. R. & Soucek, L. The long journey to bring a MYC inhibitor to the clinic. *J. Cell Biol.* **220**, e202103090 (2021).
- Habib, S., Ariatti, M. & Singh, M. Anti-c-myc RNAi-Based onconantherapeutics. *Biomedicines* **8**, 612 (2020).
- Sequera, C. et al. MYC and MET cooperatively drive hepatocellular carcinoma with distinct molecular traits and vulnerabilities. *Cell death Dis.* **13**, 994 (2022).
- Liberzon, A. et al. The molecular signatures database (MSigDB) hallmark gene set collection. *Cell Syst.* **1**, 417–425 (2015).
- Akinc, A. et al. Targeted delivery of RNAi therapeutics with endogenous and exogenous ligand-based mechanisms. *Mol. Ther.* **18**, 1357–1364 (2010).
- Bayer Healthcare. Nexavar® prescribing information (2023).
- Eisai Inc. LENVIMA® Prescribing Information (2023).

33. Mou, L. et al. Improving outcomes of tyrosine kinase inhibitors in hepatocellular carcinoma: new data and ongoing trials. *Front. Oncol.* **11**, 752725 (2021).
34. Daher, S., Massarwa, M., Benson, A. A. & Khoury, T. Current and future treatment of hepatocellular carcinoma: an updated comprehensive review. *J. Clin. Transl. Hepatol.* **6**, 69–78 (2018).
35. Wang, J. W. et al. RCN1 induces sorafenib resistance and malignancy in hepatocellular carcinoma by activating c-MYC signaling via the IRE1 α -XBP1s pathway. *Cell death Discov.* **7**, 298 (2021).
36. Jindal, A., Palejwala, V. A. & Ciomei, M. Milciclib and sorafenib synergistically downregulate c-Myc to suppress tumor growth in an orthotopic murine model of human hepatocellular carcinoma. *J. Transl. Sci.* **7**, 1–10 (2020).
37. Xia, P. et al. MYC-targeted WDR4 promotes proliferation, metastasis, and sorafenib resistance by inducing CCNB1 translation in hepatocellular carcinoma. *Cell death Dis.* **12**, 691 (2021).
38. Liu, R. et al. Gankyrin drives metabolic reprogramming to promote tumorigenesis, metastasis and drug resistance through activating beta-catenin/c-Myc signaling in human hepatocellular carcinoma. *Cancer Lett.* **443**, 34–46 (2019).
39. Merck. Keytruda[®] prescribing information (2023).
40. Bristol Myers Squibb. Opdivo[®] prescribing information (2023).
41. Genentech, Inc. TECENTRIQ[®] prescribing information (2023).
42. Casey, S. C., Baylot, V. & Felsher, D. W. The MYC oncogene is a global regulator of the immune response. *Blood* **131**, 2007–2015 (2018).
43. Casey, S. C. et al. MYC regulates the antitumor immune response through CD47 and PD-L1. *Science* **352**, 227–231 (2016).
44. Spranger, S., Gajewski, T. F. & Kline, J. MYC - a thorn in the side of cancer immunity. *Cell Res.* **26**, 639–640 (2016).
45. Principe, D. R., Chiec, L., Mohindra, N. A. & Munshi, H. G. Regulatory T-Cells as an emerging barrier to immune checkpoint inhibition in lung cancer. *Front Oncol.* **11**, 684098 (2021).
46. Watts, J. K. & Corey, D. R. Silencing disease genes in the laboratory and the clinic. *J. Pathol.* **226**, 365–379 (2012).
47. Santiago-Ortiz, J. L. & Schaffer, D. V. Adeno-associated virus (AAV) vectors in cancer gene therapy. *J. Control Release* **240**, 287–301 (2016).
48. Posternak, V. & Cole, M. D. Strategically targeting MYC in cancer. *F1000Res.* **5**, F1000 (2016).
49. McKeown, M. R. & Bradner, J. E. Therapeutic strategies to inhibit MYC. *Cold Spring Harb. Perspect. Med.* **4**, a014266 (2014).
50. Brooks, T. A. & Hurley, L. H. Targeting MYC expression through G-Quadruplexes. *Genes Cancer* **1**, 641–649 (2010).
51. Li, G. Q. et al. Suppression of BRD4 inhibits human hepatocellular carcinoma by repressing MYC and enhancing BIM expression. *Oncotarget* **7**, 2462–2474 (2016).
52. Alsouk, A. Small molecule inhibitors of cyclin-dependent kinase 9 for cancer therapy. *J. Enzym. Inhib. Med. Chem.* **36**, 693–706 (2021).
53. Alqahtani, A. et al. Bromodomain and extra-terminal motif inhibitors: a review of preclinical and clinical advances in cancer therapy. *Future Sci. OA* **5**, FSO372 (2019).
54. Tolcher, A. W., Papadopoulos, P. K. & Patnaik, A. Safety and activity of DCR-MYC, a first-in-class Dicer-substrate small interfering RNA (DsiRNA) targeting MYC, in a phase I study in patients with advanced solid tumors. *J. Clin. Oncol.* **33**, 11006 (2015).
55. Hsu, T. Y. et al. The spliceosome is a therapeutic vulnerability in MYC-driven cancer. *Nature* **525**, 384–388 (2015).
56. Lin, C. J. et al. Targeting synthetic lethal interactions between Myc and the eIF4F complex impedes tumorigenesis. *Cell Rep.* **1**, 325–333 (2012).
57. Liu, L. et al. Deregulated MYC expression induces dependence upon AMPK-related kinase 5. *Nature* **483**, 608–612 (2012).
58. Vlatkovic, I. Non-immunotherapy application of LNP-mRNA: maximizing efficacy and safety. *Biomedicines* **9**, 530 (2021).
59. Saleh, R. & Elkord, E. Treg-mediated acquired resistance to immune checkpoint inhibitors. *Cancer Lett.* **457**, 168–179 (2019).
60. Topper, M. J. et al. Epigenetic therapy ties MYC depletion to reversing immune evasion and treating lung cancer. *Cell* **171**, 1284–1300 e1221 (2017).
61. Lin, C. P., Liu, C. R., Lee, C. N., Chan, T. S. & Liu, H. E. Targeting C-MYC as a novel approach for hepatocellular carcinoma. *World J. Hepatol.* **2**, 16–20 (2010).
62. Woitok, M. M. et al. Lipid-encapsulated siRNA for hepatocyte-directed treatment of advanced liver disease. *Cell Death Dis.* **11**, 343 (2020).
63. Hou, B., Qin, L. & Huang, L. Liver cancer cells as the model for developing liver-targeted RNAi therapeutics. *Biochem. Biophys. Res. Commun.* **644**, 85–94 (2023).
64. Carabet, L. A., Rennie, P. S. & Cherkasov, A. Therapeutic inhibition of MYC in cancer: structural bases and computer-aided drug discovery approaches. *Int. J. Mol. Sci.* **20**, 120 (2018).
65. Maier, M. A. et al. Biodegradable lipids enabling rapidly eliminated lipid nanoparticles for systemic delivery of RNAi therapeutics. *Mol. Ther.* **21**, 1570–1578 (2013).
66. Ansell, S. M. & Du, X. Inventors. novel lipids and lipid nanoparticle formulations for delivery of nucleic acids. Patent application WO 2017/075531A1. (Acuitas Therapeutics, Inc., assignee, 2017).
67. Bankhead, P. et al. QuPath: open source software for digital pathology image analysis. *Sci. Rep.* **7**, 16878 (2017).
68. Patro, R., Duggal, G., Love, M. I., Irizarry, R. A. & Kingsford, C. Salmon provides fast and bias-aware quantification of transcript expression. *Nat. Methods* **14**, 417–419 (2017).
69. Lanevski, A., Giri, A. K. & Aittokallio, T. SynergyFinder 2.0: visual analytics of multi-drug combination synergies. *Nucleic Acids Res.* **48**, W488–W493 (2020).

Acknowledgements

The authors would like to thank Acuitas Therapeutics for their lipid nanoparticle formulation and continued collaboration on this project. They would also like to thank Julie Crider, PhD and Dana Barberio, MS, for medical writing and editing contributions.

Author contributions

W.S. conceptualized the studies presented in this article, coordinated the in vitro and in vivo studies, executed the in vivo studies, performed data review and interpretation, and contributed to writing. K.M.G. contributed to conceptualization of the presented studies, executed the in vitro studies, performed data review and interpretation, and contributed to writing. E.F. executed the in vitro studies and contributed to writing. J.D.F. engineered the epigenetic controllers and contributed to the selection of specific genomic location within the MYC IGD and contributed to writing. R.L. oversaw generation of mRNA material used in the in vitro and in vivo studies. J.G.H. contributed to data review and interpretation and writing. C.W.O. performed RNA-sequencing analysis, data review and interpretation and contributed to writing. M.P. generated data for resubmitted figures to address reviews and contributed to writing. J.C. generated the RNA-sequencing raw data and contributed to writing. S.S. generated the RNA-sequencing analysis and corresponding figures and contributed to writing. J.V.N. and T.G.M. contributed to conceptualization of the studies in the article, coordination of the in vitro and in vivo studies, data review and interpretation, and contributed to writing.

Competing interests

All authors were employees of Omega Therapeutics when the work was conducted. All authors were or currently are shareholders of Omega Therapeutics stock and/or options. T.G.M. is the Chief Scientific Officer of Omega Therapeutics.

Additional information

Supplementary information The online version contains supplementary material available at <https://doi.org/10.1038/s41467-024-52202-y>.

Correspondence and requests for materials should be addressed to William Senapedis.

Peer review information *Nature Communications* thanks Chen Liu, Jinjun Shi, Vlatka Zoldoš and the other anonymous reviewer(s) for their contribution to the peer review of this work. A peer review file is available.

Reprints and permissions information is available at <http://www.nature.com/reprints>

Publisher's note Springer Nature remains neutral with regard to jurisdictional claims in published maps and institutional affiliations.

Open Access This article is licensed under a Creative Commons Attribution-NonCommercial-NoDerivatives 4.0 International License, which permits any non-commercial use, sharing, distribution and reproduction in any medium or format, as long as you give appropriate credit to the original author(s) and the source, provide a link to the Creative Commons licence, and indicate if you modified the licensed material. You do not have permission under this licence to share adapted material derived from this article or parts of it. The images or other third party material in this article are included in the article's Creative Commons licence, unless indicated otherwise in a credit line to the material. If material is not included in the article's Creative Commons licence and your intended use is not permitted by statutory regulation or exceeds the permitted use, you will need to obtain permission directly from the copyright holder. To view a copy of this licence, visit <http://creativecommons.org/licenses/by-nc-nd/4.0/>.

© The Author(s) 2024